nature protocols

PROTOCOL

https://doi.org/10.1038/s41596-021-00576-4

Check for updates

High-speed laser-scanning biological microscopy using FACED

Queenie T. K. Lai[1,8], Gwinky G. K. Yip[1,8], Jianglai Wu[2,7,8], Justin S. J. Wong[1], Michelle C. K. Lo[1], Kelvin C. M. Lee[1], Tony T. H. D. Le[1], Hayden K. H. So[1], Na Ji[2,3,4,5]✉ and Kevin K. Tsia[1,6]✉

Laser scanning is used in advanced biological microscopy to deliver superior imaging contrast, resolution and sensitivity. However, it is challenging to scale up the scanning speed required for interrogating a large and heterogeneous population of biological specimens or capturing highly dynamic biological processes at high spatiotemporal resolution. Bypassing the speed limitation of traditional mechanical methods, free-space angular-chirp-enhanced delay (FACED) is an all-optical, passive and reconfigurable laser-scanning approach that has been successfully applied in different microscopy modalities at an ultrafast line-scan rate of 1–80 MHz. Optimal FACED imaging performance requires optimized experimental design and implementation to enable specific high-speed applications. In this protocol, we aim to disseminate information allowing FACED to be applied to a broader range of imaging modalities. We provide (i) a comprehensive guide and design specifications for the FACED hardware; (ii) step-by-step optical implementations of the FACED module including the key custom components; and (iii) the overall image acquisition and reconstruction pipeline. We illustrate two practical imaging configurations: multimodal FACED imaging flow cytometry (bright-field, fluorescence and second-harmonic generation) and kHz 2D two-photon fluorescence microscopy. Users with basic experience in optical microscope operation and software engineering should be able to complete the setup of the FACED imaging hardware and software in ~2–3 months.

Introduction

Innovation in laser scanning is instrumental in driving the continuing advance in modern optical microscopy, most notably in confocal and multiphoton microscopy[1]. The key rationale of laser-scanning imaging is to obtain high-contrast and high-resolution images by scanning a focused light beam onto a focal plane in the specimen with a diffraction-limited spot size. However, most available scanning techniques fundamentally lack sufficiently high imaging speed or throughput to offer plausible solutions to many challenging biological and clinical research problems. Notable challenges include capturing the fast (submillisecond) neural activities in living brains[2,3] and interrogating large populations (millions or beyond) of single cells for unraveling the intricate heterogeneity of biological systems[4–6].

To overcome this speed limitation, we recently developed an all-optical, passive and reconfigurable laser-scanning method, called FACED[7–11]. It harnesses a concept similar to an 'infinity mirror' that enables ultrafast laser line scanning at a rate well beyond MHz that is at least 10–100 times faster than galvanometric resonant mirrors, the current gold standard, and other active beam scanners, e.g., acousto-optic deflectors (AODs) and electro-optic deflectors (EODs). FACED imaging has empowered diverse imaging capabilities that were once challenging in standard microscopy, ranging from 2D full-frame voltage imaging of neural activities at kHz frame rate to single-cell imaging cytometry at a throughput of tens of thousands of cells/s. In this protocol, we showcase a wide spectrum of modalities that can be enabled by FACED. We describe how phase gradient imaging, one- and two-photon fluorescence imaging and second-harmonic generation (SHG) microscopy can be achieved at ultra-high speed without sacrificing the imaging resolution. The implementation of FACED is also compatible with a variety of imaging modalities. Hence, FACED imaging could readily

[1]Department of Electrical and Electronic Engineering, The University of Hong Kong, Hong Kong, China. [2]Department of Physics, University of California, Berkeley, Berkeley, CA, USA. [3]Department of Molecular and Cell Biology, University of California, Berkeley, Berkeley, CA, USA. [4]Helen Wills Neuroscience Institute, University of California, Berkeley, Berkeley, CA, USA. [5]Molecular Biophysics and Integrated Bioimaging Division, Lawrence Berkeley National Laboratory, Berkeley, CA, USA. [6]Advanced Biomedical Instrumentation Centre, Hong Kong Science Park, Shatin New Town, Hong Kong. [7]Present address: Chinese Institute for Brain Research, Beijing, China. [8]These authors contributed equally: Queenie T. K. Lai, Gwinky G. K. Yip, Jianglai Wu. ✉e-mail: jina@berkeley.edu; tsia@hku.hk

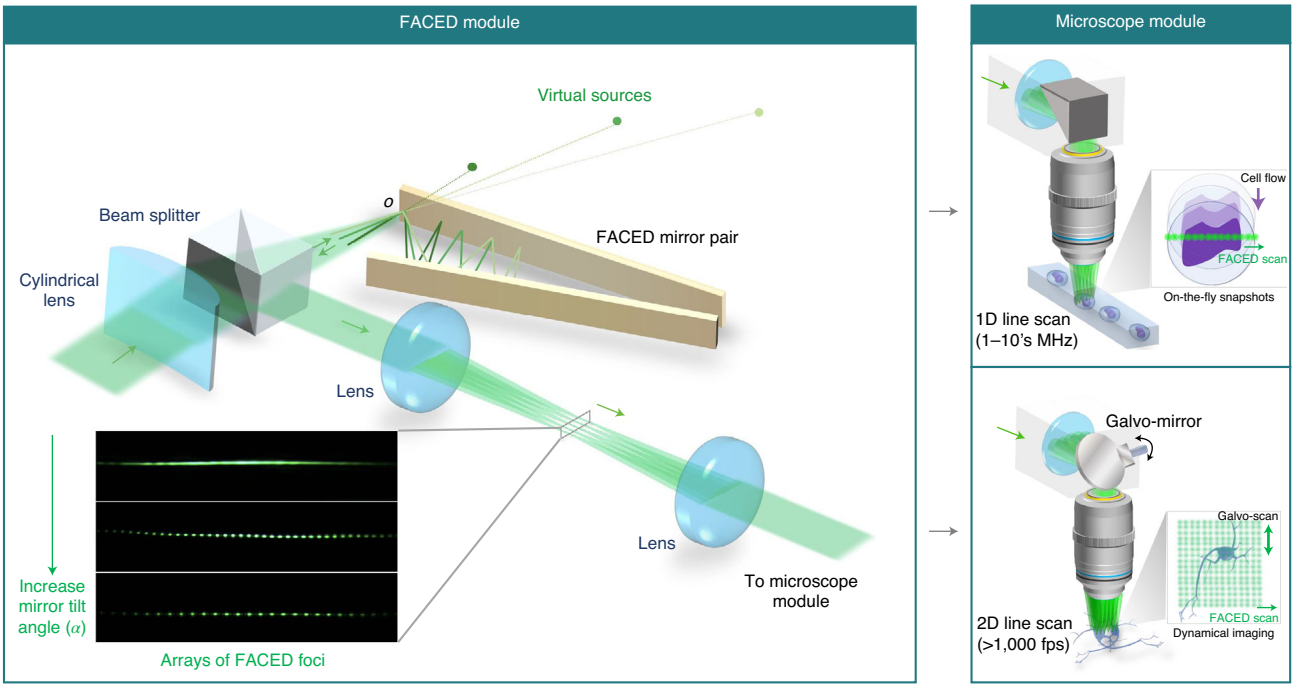

Fig. 1 | Overall schematic of a FACED microscope. The key element is a pair of almost-parallel (tilt angle α < 1 mrad) and highly reflective plane mirrors (reflectivity > 99.5%) and a focusing cylindrical lens. They transform a line-focusing pulsed laser beam (focused at entrance *O*) into a set of beamlets (only three beamlets are shown for clarity). Each beamlet follows a unique path of multiple reflections such that the corresponding zig-zag light path is progressively denser and is then retroreflected to the entrance *O* along the identical paths. The returning beamlets can be regarded as light emanating from an array of *virtual pulsed sources*. As different beamlets take different path lengths (thus time delays) from the virtual sources (depending on the incident angle at the entrance *O*), they can form an array of spatially separated and temporally delayed foci onto the imaging plane of a microscope (or any intermediate conjugate plane of the virtual sources, see the right inset) - emulating an ultrafast line-scanning beam for imaging. By tuning the geometry of the FACED mirror-pair (e.g., the tilt angle α), one can manipulate the density and number of the virtual sources (thus, foci) as shown in the left bottom corner. FACED microscopy is compatible with high-speed imaging in a 1D (static) line-scanning mode or 2D full-frame mode. The 1D mode is ideal for on-the-fly imaging applications (e.g., imaging flow cytometry), whereas the 2D mode favors real-time dynamic imaging (e.g., monitoring the spatiotemporal dynamics of neuronal signaling). In the 2D mode, an additional beam scanning module, which provides the slow-axis scan orthogonal to the FACED line scan (i.e., fast axis), is needed.

be applied to probe biological questions that are inaccessible with traditional techniques, especially those for which increased speed and throughput are beneficial.

Overview of FACED

The core components required to add laser scanning to FACED are a pair of almost-parallel plane mirrors (mirror reflectivity > 99.5% and a misaligned angle α < 1 mrad) and a focusing lens (e.g., a cylindrical lens to generate a line-focusing beam) (Fig. 1). This module splits the line-focusing pulsed laser beam (focused at entrance *O*) into a set of beamlets, each of which follows a unique zig-zag light path that has two key characteristics as a result of the angular misalignment between the mirrors: (i) each zig-zag light path is progressively denser and is retroreflected to the entrance *O* along the identical paths and (ii) the total round-trip path length, and thus the time delay for each zig-zag path, is a function of incident angle upon the entrance *O*. In essence, the returning beamlets from the mirror pair manifest themselves on emerging from an array of *virtual pulsed sources* (each has a divergence cone angle of α) (Fig. 1). When positioned between the excitation laser and a microscope, this FACED module effectively projects the virtual sources onto the focal plane of a microscope as an ultrafast line scanning beam—all-optically and passively (Fig. 1). Note that each virtual pulsed source shares the same spectral profile as the original pulsed laser source (Box 1). As a result, the information about the sample (i.e., transmitted/scattered light, fluorescence emission) is encoded to the scanning beam point by point and is detected as a temporal waveform by a high-speed photodetector.

Applications

FACED could be beneficial in a wide range of applications where high-throughput screening or high-speed monitoring is critical. Notably, the ultrafast line-scanning action makes it ideal for

Box 1 | Key design parameters of FACED

General working principle

By means of geometrical optical ray tracing, how the multiple light reflections between the two misaligned plane mirror pairs give rise to the formation of a virtual source array can be modeled. This ray-tracing model, called conjugate mirror model, serves as a handy tool to design and optimize the device's performance. First, consider an input beam focused at the entrance *O* of the FACED device by a cylindrical lens[7]. Then define a light ray within this focusing light cone and trace the subsequent multiple-reflection zig-zag path between the two mirrors. In this model, this zig-zag path can be viewed as a straight light ray passing through a series of imaginary plane mirrors (called conjugate mirrors) (Fig. 2a). Each mirror makes a tilt angle α with respect to the neighboring mirrors, forming a fan of conjugate mirrors extrapolated from the origin. C_k is denoted as the line representing the k^{th} conjugate mirror that makes a tilt angle of kα with respect to the plane of 0^{th} mirror C_0 (called principal mirror). If the two FACED mirrors have the same mirror length *L*, outer and inner circles can be defined in this conjugate mirror model, with the radii calculated with the following equation:

$$R = \frac{S}{2}\left(\sin\frac{\alpha}{2}\right)^{-1} \approx \frac{S}{\alpha} \tag{1}$$

$$r = R - L$$

where *R* and *r* is the radius of the outer and inner circles, respectively, *S* is the mirror separation and α is the angle subtended from the two mirrors. The small-angle approximation made in Eq. 1 is generally valid in the FACED device design because of the small α (< 1 mrad). One distinctive feature of a FACED device is that there is a set of zig-zag light paths, called cardinal rays, retroreflecting back along the same path to entrance *O*. In the conjugate mirror model, the light path of the k^{th} cardinal ray (incident at *O* with an angle *q*), intersects with *k* intermediate conjugate mirrors (i.e., the light experiences *k* mirror reflections) before it is normally incident to the conjugate mirror C_k and is retroreflected back to the entrance *O* along the same path. This path can also be viewed in an alternative way, with the light emerging from a virtual point (O_k), which is, in essence, the virtual image point of the entrance *O* with respect to the conjugate mirror C_k, (i.e., located at the intersection of the conjugate mirror C_{2k} and the rim of the outer circle in the ray tracing diagram shown in Fig. 2b**)**. Geometry[7] proves that the incident angle of the k^{th} cardinal ray is an integer multiple of mirror tilt angle (i.e., $\theta_k = k\alpha$). The incident light rays that do not satisfy the condition of the cardinal rays still follow similar zig-zag paths and are retro-reflected, but without following the original incoming path. Specifically, the light rays that deviate from the k^{th} cardinal ray but experience the same number of mirror reflections (a total of 2*k* reflections in a round trip) can be viewed as if they emerge from a virtual point O_k (see Fig. 2b). As each of the virtual sources locates at a different distance away from the entrance *O*, there is a time delay τ between two neighboring cardinal rays arriving back at *O*. This is calculated by the following equation:

$$\tau = \frac{2R}{c}[\sin(k+1)\alpha - \sin k\alpha] \approx \frac{2S}{c} \tag{2}$$

where *c* is the speed of light in free space. Overall, by virtue of the multiple reflections between the misaligned mirror pair, the FACED device transforms a single pulsed beam into a set of beamlets that emerge from an array of virtual (point) sources. As the virtual sources are spatiotemporally separated, they are projected onto the image plane through intermediate microscope optics as a laser line-scanning beam without relying on any mechanical scanning mechanism. It should be noted that each virtual source shares the same original bandwidth and, thus, the transform-limited temporal pulse width of the input laser source. This is different from another FACED configuration based on spectral encoding[7], in which a spectrally resolvable spot only shares a narrow band of the entire source spectra and thus has a much broader temporal pulse.

NA of a FACED device

There is an upper limit of incident angle (θ_{max}) at the entrance *O*, beyond which the light ray escapes from the far end of the device, instead of retroreflecting back. This is the situation when the project light ray enters the inner circle of the conjugate mirror model (Fig. 2a). It refers to $R\cos\theta_{max} \geq r$. An NA of the device can thus be defined that describes the maximum acceptance input cone angle within which the light rays can be back reflected:

$$NA = \sin\frac{\theta_{max}}{2} \approx \sqrt{\frac{1 - r/R}{2}} \tag{3}$$

Clearly, NA is governed by the physical dimensions of the FACED device, including *S*, *L* and α. It also sets the maximum number of virtual sources N_{max} supported by the FACED device, which is expressed as

$$N_{max} = \frac{\theta_{max}}{\alpha} = \sqrt{\frac{2L}{S\alpha}} \tag{4}$$

In general, N_{max} increases with smaller mirror separation, smaller tilt angle and longer mirror length. In practice, it is preferable to set the input light cone angle to be smaller than θ_{max}, (i.e., $\Delta\theta < \theta_{max}$), which is discussed in further detail in 'Experimental design'; the corresponding number of cardinal rays is simply $N = \Delta\theta/\alpha$. This cone angle can be adjusted by the focal length of the cylindrical lens f_{cyl} and the input laser beam size w_o, i.e., $\Delta\theta = w_o/f_{cyl}$.

Projection of virtual sources

The virtual sources, each of which has a divergence angle of α, is typically imaged by a lens (L2 in Fig. 3) and is projected to the immediate conjugate plane, which is a critical position to evaluate the quality of the projected virtual sources. Given that the distance between the k^{th} virtual source and the lens L1 is $OL_k \approx f_2 + 2kS$ (based on paraxial approximation as NA of the FACED device ≪1), the corresponding image of the virtual source locates at

$$IL_k \approx f_2\left(1 + \frac{f_2}{2kS}\right) \tag{5}$$

Box 1| (continued)

after the lens L2. Thus the virtual sources are imaged at different image planes/depths. However, in many imaging scenarios, it is desirable to ensure all the virtual sources illuminate/excite the imaged sample within the depth of field of the microscope. Placing an aperture stop on the immediate conjugate image plane to select the 'high-order' virtual sources (i.e., larger k), among which the difference between their focal distances is relatively small, achieves this. The f_2, k and S should be carefully manipulated to minimize the difference between IL_k and IL_{k+1} (Eq. (5)).
The fact that each beamlet originated from its virtual source has a different beam size at the back focal plane of the objective lens has an impact on the further projection of the virtual source array to the image plane of the microscope. As the size of the beamlet from the k^{th} virtual source at the lens L2 can be approximated as $W_k \approx \alpha \times OL_k$, the beamlet size projected at the back focal plane of the objective can be expressed as $M{\cdot}W_k$, where M is the magnification of the intermediate relay optics (e.g., in the configuration shown in Fig. 3, $M = (f_3/f_2){\cdot}(f_{TL}/f_4)$). Note that that the beamlet size (BS_k) mentioned here refers to the fast-axis direction (x-direction), whereas the beamlet size along the slow axis (y-direction) of each k^{th} virtual size can be estimated as

$$W_{y,k} = 2M\,w_y = 2M\,w_o\sqrt{1+\left(\frac{\lambda\,OL_k}{\pi w_o^2}\right)^2} \tag{6}$$

where w_o is the original beam waist before entering the cylindrical lens. Since the beamlets have different sizes at the objective aperture, the resultant scanning foci have different effective NA and, thus, different focal spot size. Hence, this effect could influence the image resolution, which is discussed in more detail in 'Spatiotemporal resolution of the FACED microscope'.

Optical loss of FACED
The key intrinsic loss of FACED is attributed to the less-than-unity mirror reflectivity R. Assuming both mirrors have the same reflectivity and considering the total incident power is uniformly distributed across the incident beam profile (across the N virtual sources), the intrinsic loss of the FACED mirror pair can be estimated by tracing the number of reflections of all the cardinal rays (Fig. 2a):

$$Loss = \frac{1}{N}\left(1+R^3+R^5+\cdots+R^{2N-1}\right) = \frac{1}{N}\frac{R\left(1-R^{2N}\right)}{1-R^2} \tag{7}$$

Loss $\approx R^N$ when R approaches 1 for large N. This condition is generally true in many FACED configurations in which the reflectivity $R > 0.995$ and N is typically $\gg$10 (refs. [7–11]). We note that any other angles θ' that deviate from θ_k will make a total of $2\lfloor\theta'/\alpha\rfloor$ mirror bounces to ensure the beamlet is retroreflected, where $\lfloor\bullet\rfloor$ is a floor function. Based on this condition, all the light rays (in continuum) within the input light cone can be traced as if they emerge from an array of discrete virtual point sources. In essence, the input beam is reshaped by the FACED mirror pair into a beamlet array. There is no optical loss during this 'reshaping' process, except the non-unity mirror reflectivity (see Eq. (7)).

high-throughput imaging cytometry in the 'on-the-fly' configuration, i.e., either imaging suspended cells in fast microfluidic flow[12] or adherent cells/tissues[7–9] on a solid platform (e.g., spinning disk)[13]. We have developed a FACED imaging flow cytometer for investigating the subcellular morphological changes of lysosome-labeled cells during both starvation-induced and drug-induced cell death at an imaging throughput of 75,000 cells/s[8]— at least two orders of magnitude higher than the current camera-based imaging flow cytometers. A similar FACED imaging flow cytometer (with both bright-field and fluorescence image contrasts) has been employed to classify and analyze a cancer cell population spiked into a heterogeneous human blood sample[9]. As FACED can be readily adapted for use in any imaging modalities that are compatible with the laser-scanning operation, FACED imaging cytometry could be used to extract a variety of richer phenotypic information about individual cells. For instance, quantitative phase imaging cytometry[14–21] has been demonstrated to enable biophysical phenotyping of single cells (such as cell mass, size and subcellular morphology/textures) for label-free drug screening[22], cancer diagnosis[23–25], blood screening[26,27] and microalgal culture evaluation[16,18]. Therefore, FACED imaging cytometry could represent a powerful tool for exploiting and integrating all the relevant phenotypic data for individual cells at a throughput and content level that are not achievable or affordable with current cell-based imaging technologies. This is a critical attribute required in all single-cell analysis tools for deciphering the complex biological processes, especially in unveiling unknown cellular heterogeneity[28] and thus uncovering new biomarkers of health and disease[29].

Combined with a standard galvanometric or resonant scanning mirror that provides a 'slow axis' scan orthogonal to the FACED scanning beam ('fast axis'), FACED is well suited for high-speed 2D full-frame microscopy beyond 1,000 frames per second (fps). For example, 2D FACED fluorescence microscopy has been applied to observe kHz photothermal modulation in cell size[9]. Recently, kHz two-photon fluorescence microscopy (2PFM) based on FACED has been demonstrated (1,000–3,000 fps) to monitor spontaneous and sensory-evoked suprathreshold and subthreshold electrical activities using the genetically encoded voltage indicator (ASAP3) down to >300 μm below the brain surface in head-fixed awake mice[11]. The same FACED 2PFM system could also be used to monitor transient neural activities with calcium indicators (e.g., GCaMP6[30]) and glutamate sensors (e.g., iGluSnFR[31]) at

subcellular resolution. Hence, alongside the continuing advances in brighter and faster genetically encoded indicators, FACED multiphoton microscopy could open a new avenue in the full-frame kHz-rate recording of neural signaling at synaptic and cellular resolution in vivo—the key to dissecting the complex mechanisms of neural activity in intact brains of behaving animals.

Furthermore, we anticipate that laser-scanning microscopy based on FACED can further be extended to high-speed volumetric imaging (video volume rate or beyond) when it combines with an additional axial scanning mechanism. A promising example involves remote focusing based on a tunable acoustic gradient index of refraction lens[32,33]. In addition, we have recently extended the concept of FACED to enable parallelized 3D light-sheet fluorescence imaging in scattering media, optically cleared tissue structures, and microparticles in microfluidic flow at a 3D imaging rate of >10 vol/s[10]. In virtue of its full 3D parallelization, this technique will be of particular interest in long-term, live imaging that requires a minimal risk of photobleaching and photodamage.

Comparison with other methods

Currently, the vast majority of the laser-scanning imaging modalities adopt the raster point scanning approach for 2D/3D image capture. Galvanometric and resonant mirrors are among the most popular choices. However, fundamentally limited by mechanical inertia, the 1D scan rate of these scanners can typically be up to ~1–10 kHz. This results in a 2D frame rate of tens of fps (e.g., ~45 Hz at 512 × 512 pixels for a 12 kHz resonant scanning mirror)[34]. Further speed improvement could be made by the rotating polygonal mirror, which can scale the speed up to ~100 kHz[35]. Scanners based on AODs and EODs, on the other hand, are not subject to the mechanical inertia and instability and can thus operate at a faster scan rate of hundreds of kHz, at the expense of the angular scanning range and the number of resolvable scan points[36]. In addition, AOD and EOD are intrinsically dispersive elements that disperse and distort the ultrafast broadband beams used for multiphoton excitation, thus requiring careful dispersion compensation, which increases system complexity and limits its widespread utility in common confocal and multiphoton imaging systems. Another approach for high-speed laser scanning is spectral encoding based on a wavelength-sweep concept[37]. Notably, this all-optical laser scanning approach can achieve a scan rate of up to tens of MHz by optical time stretch[18,38,39]. Despite its ultrafast rate, laser-scanning fluorescence microscopy using spectral encoding is regarded as spectrally inefficient because only a narrow band of the entire source spectra is used for fluorescence excitation on each spectrally resolvable spot. To achieve high-resolution fluorescence microscopy, this technique is required to obtain sufficiently large dispersion, which inevitably leads to high optical loss. The dispersive loss can be mitigated by a high-speed wavelength-swept source combined with a master oscillator power amplifier, which has recently been demonstrated to achieve a sub-MHz repetition rate for enabling kHz 2PFM[40]. It should be noted that spectral encoding can also be implemented in FACED when the input cylindrical lens is replaced by a diffraction grating. In this case, FACED operates as an optical time-stretch device—in which the mirror pair functions as a highly dispersive medium that temporally stretches the subpulses. Again, such a spectral encoding scheme might not be spectrally efficient for fluorescence imaging. While this is not the implementation described in this protocol, interested readers can refer to ref. [7] for more details.

In contrast, laser-scanning imaging using FACED offers several advantages over the aforementioned techniques:

(i) *Imaging speed*: FACED bypasses the use of active beam scanners and their speed limitations to achieve a line-scan rate beyond 1–10 MHz, determined by the repetition rate of the pulsed laser. This is a passive, all-optical technique that is at least 10–100 times faster than AOD or EOD, and 100–1,000 times faster than mechanical galvanometric/resonant mirrors.

(ii) *Reconfigurability and scalability*: the total number of virtual sources N (i.e., scan spots), the angular scan range (thus, field of view (FOV)) and the spatial and temporal separation between the neighboring virtual sources can be scaled flexibly by adjusting the geometry of the FACED mirror module (Figs. 1 and 2) (e.g., mirror separation, misaligned mirror angle and numerical aperture (NA) of the input light cone; see Box 1). For example, in one of the previous demonstrations, we generated $N = 80$ with a neighboring temporal separation of 2 ns[11] whereas another configuration created $N > 150$ with a temporal separation of 100 ps[7].

(iii) *Scanning beam quality*: the free-space retroflection property of FACED introduces no distortion in the shape of each virtual source, and thus ensures diffraction-limited scan spots across the

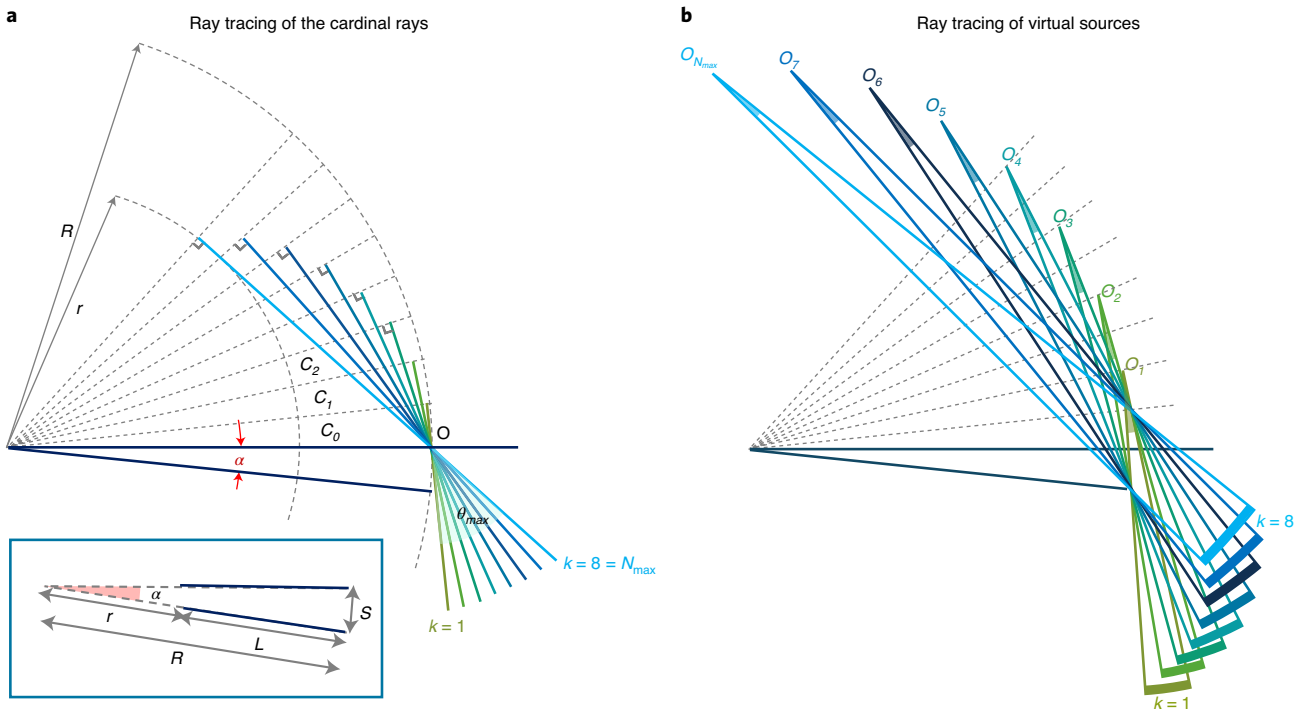

Fig. 2 | Ray-tracing diagram of a FACED device based on a conjugate-mirror model. a, Cardinal rays. Conjugate mirrors[7], defined as the images of the adjacent mirror (dashed lines). An incident light cone focuses onto the entrance *O* of the FACED device. The light propagation characteristics in the device can be understood by 'unfolding' the multiple reflection paths and viewing them as a set of straight rays intersecting with the conjugate mirrors. These rays, called cardinal ray ($k = 1...8$ in this figure), intersect orthogonally with the conjugate mirrors and are retroreflected back to entrance *O* along the same paths. The point at which the ray tangentially touches the inner circle (radius of *r*) represents the furthest point that the light is allowed to be retroreflected back to entrance *O* along the same path. The angle between the first and eighth cardinal rays represents the acceptance angle $\theta_{max} = N_{max}\alpha$ of the device. N_{max} is the maximum number of cardinal rays (or virtual sources) supported by the device. The left bottom inset shows the geometrical parameters defined for the FACED device. **b**, Virtual sources. O_k is the conjugate image point of *O* with respect to C_k, i.e., the virtual source. All other light rays within the same light cone can still be retroreflected, but not along the identical paths. The overall returning light is transformed into an array of beamlets, which can be viewed as light emanating from an array of spatiotemporally encoded virtual sources (each has a divergence cone angle of α). For the k^{th} virtual source, there are the upper and lower bound of the light rays such that they are still subject to the same number of mirror reflections (*k* in this case) as that of the *k*th cardinal ray.

entire virtual source array. Unlike AOD and EOD, the free-space, wavelength-independent operation of FACED introduces no dispersion and minimal loss (because of high mirror reflectivity) to the ultrafast broadband pulses. This is particularly critical in the scenarios where photon budget is limited, especially one-photon fluorescence or multiphoton excitation.

(iv) *Adaptability*: as a passive optical module simply based on a pair of high-reflectivity plane mirrors, FACED can be easily incorporated into existing microscopes (in different imaging modalities and contrasts, e.g., bright-field, phase-contrast, one-photon fluorescence, multiphoton) to enable high-speed laser scanning with minimal hardware or software modification.

Caveats and limitations

The main caveat and limitation of FACED is the loss of signal-to-noise ratio (SNR) at high laser-scanning speed, i.e., dwell time per scan spot is reduced at higher scan speed. Guided by the available photon budget for different imaging modalities, a strategic compromise must be made for each imaging scenario between imaging speed, resolution, photodamage/photobleaching and other experimental settings (e.g., 1D, 2D or 3D imaging mode, sample size, imaging duration). Our previous work showed that it is necessary to achieve a data acquisition rate of beyond 1 GSample/s (or 1 GB of data per second). For continuous data recording for more than minutes, traditional offline processing of imaging information is challenging owing to the sheer amount of effort required for data transfer. High-performance data processing in situ is required as data are generated from the imaging front end. Nevertheless, the computational procedure details we provide can be adopted without the need for expert knowledge in hardware computation design and engineering.

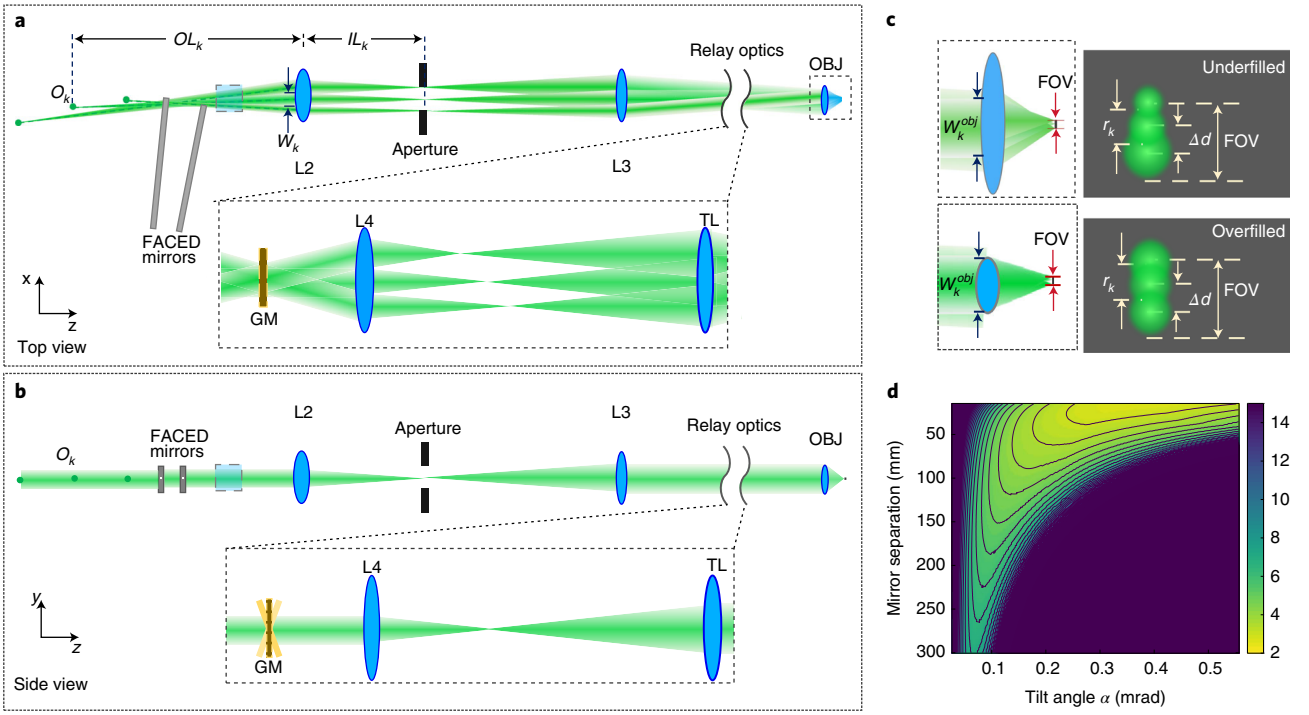

Fig. 3 | Design considerations for FACED imaging. a,**b**, Top view (**a**) and side view (**b**) of the ray tracing of the beamlets emerged from the virtual sources in the FACED setup. **c**, Zoom-in views of the beamlets passing through the objective in two cases: the objective is (top) underfilled and (bottom) overfilled with each beamlet. **d**, Contour map of *P1* + *P2* (see Eqs. (11–13)) for the targeted configuration of FACED: $N = 100$, and FOV = 50 mm. This map can be used to search for the best practical combinations of S, α and M in the vicinity of the minimum *P1* + *P2*. L2, L3, L4, spherical lens; TL, tube lens; OBJ, objective lens; GM, galvo mirror.

Experimental design

Here we discuss the key experimental design rules of the FACED module and the imaging systems (Fig. 3), before discussing the equipment required.

Key specifications of FACED

Once the research question to be addressed and the choice(s) of imaging contrast have been determined, the required spatial resolution, imaging FOV and targeted imaging frame rate should be defined. These are the key criteria for guiding the design of the FACED module as well as the microscope configuration. The major design specifications of the FACED module include the misaligned angle of the mirror pair (α), mirror-pair separation (S), length of the mirrors (L) and input light beam condition (see the design theory in Box 1). On the other hand, the relevant specifications of the microscope include total magnification (of the relay optics between the virtual sources and the sample plane), and the NA of the objective lens. The overall rationale is to identify the optimal combinations of all these design parameters that generate the scanning beam profiles on the sample plane with the desired spatiotemporal resolution and FOV, for a given targeted line-scan rate (1/T). As discussed later, this design process can be implemented simply according to the concept of geometrical optics, in which the beam profiles can be evaluated analytically or through a numerical ray-tracing simulation tool (e.g., Zemax OpticStudio).

Generation of all-optical laser-scanning beam by FACED

Construction of the FACED module requires the basic skillsets of optical system alignment, including lens and mirror alignment and focal plane detection. The practical guide by R. Heintzmann[41] provides additional guidance on implementing these stages. In general, the goal is to ensure minimal aberration, distortion and tilt in the virtual source array projected from the mirror pair on the intermediate conjugate plane. This requires iterated adjustments of the input cylindrical lens position, the tilt (yaw) and pivot (pitch) angles of the FACED mirrors (see the steps in 'FACED module setup and calibration').

With its optimal beam profile, the virtual source array at the intermediate conjugate plane can then be projected through an infinity-corrected microscope system (mainly with a tube lens (TL) and an objective lens) (Fig. 3a,b). An additional module of telecentric lenses is typically needed to further resize the arrayed beamlets before the microscope. The spatial profile of the excitation/illumination scanning beamlets (foci) on the sample plane can be imaged and assessed by a camera of the microscope. The temporal profile can, on the other hand, be captured and evaluated by a large-area photodetector (i.e., photodiode or photomultiplier tubes (PMTs), depending on the chosen imaging modalities).

Another point to note is that the scanning foci across the line scan are the images of virtual sources located at increasing distances away (Box 1). Thus, the foci are actually at different depths. Nevertheless, using an aperture stop, a subset of the whole virtual-source array can be selected such that the virtual sources can be imaged within the depth of focus of the infinity-corrected microscope (Fig. 3a,b). This selection requires a balance between image quality (i.e., maximally uniform focal spot size across the array), photon budget (i.e., avoiding excessive optical loss by the aperture stop), and imaging FOV (i.e., maximize the number of virtual sources used for illumination). Iterated adjustments of both the FACED module and the microscope alignments should enable the best optimal laser-scanning profile to be determined. The detailed steps required for these alignments are described in 'FACED module setup and calibration'.

Spatiotemporal resolution of the FACED microscope

The spatial resolution of the FACED microscope is strongly influenced by the profile of scanning foci, especially along the FACED axis (i.e., fast axis). Here we describe the general design rules for matching the targeted spatial resolution and FOV. First of all, we consider the most common imaging scenario in which the densely packed scanning foci is employed. In this case, the spatial separation between adjacent foci (Δd) should be equal to or smaller than the resolution according to the Rayleigh criterion, i.e., $r = 0.61\lambda/NA_{obj}$, where λ is the illumination wavelength and NA_{obj} is the NA of the objective lens. We can then estimate the required number of scan spots with the targeted FOV along the FACED axis, i.e., $FOV = \Delta\theta \cdot f_{obj}/M$, where $\Delta\theta$ is the input cone angle incident onto the FACED mirror pair; f_{obj} is the focal length of the objective lens; and M is the beam-size (de)magnification factor by the intermediate relay optics (between the FACED mirror pair and the objective lens). The number of scan spots N can be evaluated as

$$N \approx \frac{FOV}{\Delta d} = \frac{\triangle\theta \cdot f_{obj} \cdot NA}{0.61\lambda \cdot M} = \frac{\triangle\theta \cdot D_{obj}}{1.22\lambda \cdot M} = \frac{w_0 \cdot D_{obj}}{1.22 f_{cyl} \cdot \lambda \cdot M} \quad (8)$$

where $D_{obj} \approx 2 f_{obj}\, NA$ is the aperture size of the objective lens. Note that the cone angle is determined by the input beam size (w_0) and the focal length of the cylindrical lens CL1 (f_{cyl}), i.e., $\Delta\theta = w_0/f_{cyl}$. Hence, Eq. (8) describes the proper specifications of the objective lens (D_{obj}, f_{obj}, NA), the combination of the relay optics (i.e., the magnification factor M) and the input beam cone angle ($\Delta\theta$) for achieving the targeted N. We note that the cone angle should be smaller than the NA of the FACED mirror pair, $\Delta\theta < \theta_{max}$, to prevent light leakage from the far end of the mirror pair (Box 1). This is equivalent to satisfying the condition of $N < N_{max}$ (see Eq. (4) in Box 1)

Apart from the spatial consideration, the temporal characteristics of the laser source and photodetector also influence the choice of N and, thus, temporal separation (delay) between the neighboring virtual sources τ (Eq. (2) in Box 1). Specifically, there is an upper limit of N beyond which the adjacent line scans overlap with each other in time. Given that the laser pulse width τ_{laser} is much shorter than the τ (sub-ps to 10 ps), i.e., $\tau_{laser} \ll \tau$; and the detector bandwidth B (e.g., 5–10 GHz) is also wide enough to resolve the adjacent foci in time (e.g., 200 ps to 2 ns), i.e., $\tau \gg 0.35/B$ assuming a 10–90% rise time of the photodetector, the upper limit of N is then determined by the repetition rate of laser 1/T and the targeted τ, i.e., $N\tau \leq$ T. The temporal separation between virtual sources τ can directly be controlled by tuning the spatial separation of the mirror pair (see Eq. (2)) to tailor different imaging modalities. For instance, in the case of bright-field and SHG imaging, τ is largely limited by the bandwidth of the photodetector and the sampling rate of the digitizer. On the other hand, to implement one- and multiphoton fluorescence microscopy, τ has to be wide enough to minimize the crosstalk between adjacent virtual sources due to the fluorescence decay in time, which is typically in the order of >1 ns (i.e., S > 150 mm) for most of the fluorescence labels used in bioimaging. Hence, the temporal resolution is primarily limited by the fluorescence lifetime. Note that the time delay τ scales with the physical footprint of the FACED module (as well as the susceptibility in optical misalignment) because larger mirror separation is required. For multiphoton imaging applications,

one should take extra care of the potential pulse broadening (thus, peak power loss and degraded image quality) due to the mirror dispersion. As a general rule of thumb, the mirror should have a low group delay dispersion (GDD) of <10 fs^2 to minimize pulse broadening for an input pulse width of <100 fs. In this case, an additional module of pulse compressor with a reconfigurable GDD is essential (typical range of GDD should be ~10,000 fs^2). On the one hand, GDD can be optimized by characterization of the ultrashort pulse width and shape using an autocorrelator. On the other hand, it would be more direct to tune the GDD directly guided by the acquired image quality (which can be done in real time as described in our protocol). In the case of linear imaging, the requirement for ultrashort pulses can be relaxed (e.g., picosecond pulse can be used). It thus makes the pulse broadening effect less substantial.

Having defined N, which N virtual sources should be used for illuminating/exciting the imaged sample needs to be further refined. As discussed, the virtual sources, from first to last, are imaged onto different image depths (Fig. 3a,b). Hence, it is necessary to identify those N virtual sources defined in Eq. (6) that could be focused within the depth of field of the objective lens (Box 1). They correspond to the 'high-order' group (i.e., larger k), starting from the ${k_{start}}^{th}$ virtual source to the highest-order virtual source (i.e., ${N_{max}}^{th}$), such that $N = N_{max} - k_{start} + 1$ (see the discussion related to Eqs. (12–13)). In practice, it could simply be done by placing an aperture stop on the immediate conjugate plane or adjusting the incident and total cone angle of the input beam to select these 'high-order' virtual sources. One should be aware that the first method could induce relatively higher power loss when the maximum number of virtual sources $N_{\max}$ (typically beyond 100 or even 200) is much larger than the selected N number of virtual sources, while the second method will not induce substantial power loss. Note that an iterated search for the optimal specifications of the FACED devices, relay optics and objective lens is necessary for this step.

So far, it has been assumed that all the beamlets overfill the back aperture of the objective lens, i.e., the full NA of the objective lens is used. However, the lower-order (less distant) virtual sources could result in underfilling the back focal plane of the objective lens, thus implying larger foci along the fast axis (Fig. 3c). Note that the beamlets generally filled the back focal plane more along the slow axis than the fast axis. In the scenario where the k^{th} beamlet underfills the objective lens with a beam size given by $W_k^{obj} \approx M \cdot \alpha \cdot OL_k$ (Box 1), the spot size of the k^{th} virtual source focused by the objective lens can be defined as $r_k = 0.61\lambda/NA_k^{eff}$. Here, NA_k^{eff} is the effective NA of the k^{th} focus spot and is estimated as $NA_k^{eff} = W_k^{obj} \cdot M/2f_{obj}$. Accordingly, the spot size can be evaluated as

$$r_k = 0.61\frac{2f_{obj}\lambda}{W_k^{obj}\cdot M}, \quad \text{when } NA_k^{eff} < NA_{obj} \tag{9}$$

Note that Eq. (9) refers to the spot size along the fast axis, whereas the spot size along the slow axis (y-direction) can be expressed as

$$r_y = 0.61\frac{2f_{obj}\lambda}{W_{y,k}^{obj}} \tag{10}$$

where $W_{y,k}^{obj} = 2M\,w_y = 2M\,w_o\sqrt{1+\left(\frac{\lambda\,OL_k}{\pi\,w_o^2}\right)^2}$ is the estimated k^{th} beamlet size along the slow axis.

To identify the optimal specifications holistically, define two dimensionless parameters that could guide the design to identify the optimal resolution and FOV. The first parameter is defined as $\boldsymbol{P_1}$, which is the ratio of the averaged focus spot size ($\bar{r}$) to the separation between neighboring foci (Δd). Depending on the beamlet filling condition at the back focal plane the objective (as shown in Fig. 3c), $\boldsymbol{P}_1$ can be expressed as

$$\boldsymbol{P}_1 = \frac{\bar{r}}{\Delta d} = \begin{cases} 0.61\frac{\lambda}{\Delta d\cdot NA_{obj}} & \text{(overfill)} \\ 0.61\frac{\lambda}{\Delta d\cdot NA_{eff}} = 0.61\frac{\lambda}{\bar{k}\cdot S\cdot\alpha^2} & \text{(underfill)} \end{cases} \tag{11}$$

Here the foci separation is evaluated by $\Delta d \approx FOV/N = FOV\cdot\alpha/\Delta\theta = \alpha f_{obj}/M$, and $\bar{k} = \left(N_{max} + k_{start,max}\right)/2$. Another dimensionless parameter is defined as $\boldsymbol{P_2}$, which describes the size ratio of the ${k_{\text{start}}}^{\text{th}}$ to the ${k_{\text{end}}}^{\text{th}}$ beamlet at the back focal plane of the objective ($k_{end} = k_{start} + N - 1$), i.e.,

$$\boldsymbol{P}_2 = \frac{W_{k_{end}}^{obj}}{W_{k_{start}}^{obj}} = \frac{k_{start} + N - 1}{k_{start}} \tag{12}$$

The k_{start}^{th} virtual source is chosen to minimize the transmission loss through the aperture of the objective and depends on two conditions:

$$k_{start} = \begin{cases} \frac{D_{obj}}{2S\alpha M}, & when\ W^{obj}_{k_{start,max}} \geq D_{obj} \quad \text{(overfill)} \\ k_{start,max}, & when\ W^{obj}_{k_{start,max}} < D_{obj} \quad \text{(underfill)} \end{cases} \tag{13}$$

where $k_{start,max}=N_{max}-N+1$, W^{obj}_{k} is the beamlet size of the k^{th} virtual source at the back aperture of the objective. Note again that W^{obj}_{k} increases with k (i.e., the virtual source order). Hence, if the $k_{start,max}^{th}$ beamlet already overfills the back aperture of the objective (i.e., $W^{obj}_{k_{start,max}} \geq D_{obj}$), the 'lower-order' starting virtual source such that the corresponding beamlet just completely fills the objective aperture should be searched for, i.e., $W^{obj}_{k_{start}} = D_{obj}$. Otherwise, choose the last N virtual sources, i.e., starting from the $k_{start,max}^{th}$ to the N_{max}^{th}.

In general, we recommend that the averaged focus spot size and the separation between neighboring foci are as similar as possible (i.e., $\boldsymbol{P}_1$ close to unity) so as to ensure optimal sampling. Also, the beam size difference between the k_{start}^{th} beamlet to the k_{end}^{th} beamlet at the back aperture of the objective should be minimized (i.e., $\boldsymbol{P}_2$ should be as small as possible). On the one hand, this could reduce image aberration such as field curvature and distortion. On the other hand, this could reduce power loss when all N virtual sources overfill the objective lens. These considerations can be formulated as identifying the conditions that minimize $\boldsymbol{P}_1 + \boldsymbol{P}_2$. The conditions are referred to as the optimal combinations of the FACED device's geometry (especially S and α), magnification of the relay optics (M) and, therefore, the input beam condition (w_o and f_{cyc}). Based on the targeted imaging specifications (N, FOV, $1/T$), the design procedures should involve a tradeoff analysis that searches for the best practical combinations of S, α and M in the vicinity of the minimum $\boldsymbol{P}_1 + \boldsymbol{P}_2$ (Fig. 3d), to achieve the desired (practical) spatiotemporal resolution and image quality.

Mechanical stabilization of the FACED mirror pair

In general, we have found that that many off-the-shelf kinematic mounts or platforms offer rigid mechanical support, providing adequate stability to hold the FACED mirror pair in place. These mounts also allow sensitive and reproducible tip and tilt adjustment of the mirror pair for precision optical alignment. Nevertheless, for continuous and long-term experiments (beyond 10 min and up to several hours), we recommend including an active feedback mechanism to stabilize the mirror pair. This could be done by setting up an additional laser-beam position sensor along the beam path (after the FACED mirror pair) and tracking the FACED beam position in real time. The tracked position can be used to correct the slow drift in the kinematic mounts, especially in the pitch direction (Supplementary Manual 1). We found that this active stabilization is favorable for robust experiments that take >10 min.

Microscope hardware setup and operation

As the FACED device is a passive optical module based on high-reflectivity plane mirrors and off-the-shelf optical components, it is readily compatible with many existing microscopes (in different imaging modalities and contrasts) to allow high-speed laser-scanning performance. Therefore, the overall imaging hardware architecture of the FACED microscope is generally identical to a traditional optical microscope (in both the transmission and reflection configuration). The essential common components include objective lenses, TLs, spectral filters (depending on different image contrasts) and photodetector (e.g., high-speed photodiode or PMT). However, there are two main considerations that are specific to the FACED microscope operation. First, the FACED microscope works well for high-speed imaging in a 1D (static) line-scanning mode or 2D full-frame mode. The 1D mode is ideal for on-the-fly imaging applications (e.g., imaging flow cytometry), whereas the 2D mode favors real-time dynamical imaging (e.g., monitoring the spatiotemporal dynamics of the neuronal signaling). The key difference between the two operation modes is that an additional beam scanning module, which provides slow-axis scanning orthogonal to the FACED line scan (i.e., fast axis), is needed in the 2D mode. The overall 2D full-frame speed in this case is governed by the scanning speed along the slow axis. For instance, a galvo-mirror (GM) scanning at 0.5 kHz directly translates to a 2D frame rate of 1,000 fps. This additional scanning module (consisting of the GM/resonant mirror and relay optics for adjusting the beam size) should be positioned between the FACED device and the illumination objective lens of the microscope (Fig. 1). Second, special care has to be taken to minimize the optical loss due to the aperture size mismatch with the FACED beam. More precisely, it must be ensured that the finite apertures of all the intermediate optics between the FACED device and the

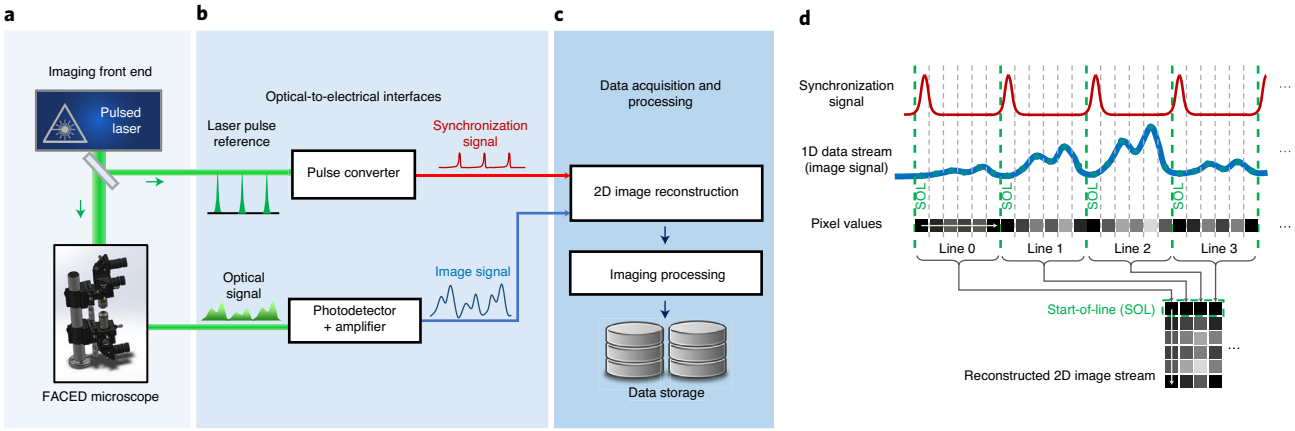

Fig. 4 | Overview of FACED image acquisition flow diagram. a, Imaging front end—FACED cavity and the relay optics. **b**, Optical to electrical interface. **c**, Data acquisition and processing. **d**, Working principle of the 2D image reconstruction.

sample plane can cover the projected FACED beamlets. This requires careful design of the magnification of the intermediate relay optics, which could also influence the desired image resolution, as discussed in the previous section. In the procedure, we provide detailed instructions for three example implementations:

- A 1D mode generating the bright-field/phase-gradient and (one-photon) fluorescence contrast
- A 1D mode generating the bright-field and SHG contrast
- A 2D mode generating the two-photon fluorescence contrast

The first two (1D) systems use a microfluidic flow platform, in which single cells are flowing in a single direction orthogonal to the FACED line scan. The last system (2D) describes 2PFM of in vivo neural activity of a living mouse.

Image acquisition, reconstruction and processing pipeline

Two different approaches can be implemented for data acquisition with different hardware, image processing and storage pipelines: (i) a high-bandwidth real-time oscilloscope (Step 65A) and (ii) a custom field-programmable gate array (FPGA) image acquisition and computing platform (Step 65B). Both approaches share the same general image acquisition and processing flow as summarized in Fig. 4a–c. The workflow starts from the FACED imaging front end, the optical-to-electrical signal conversion (for both the synchronization and the image recording purposes), which is followed by the image reconstruction, processing and storage operations.

Both approaches share the same basic principle of image reconstruction (Fig. 4d). Pixels are sampled from the image signal stream at discrete time intervals to form a continuous 1D stream of pixels, while the synchronization signal generated from the reference laser pulses defines the 'start-of-line' (SOL) position that allows the 1D stream of pixels to be subdivided into lines of pixels with an equal length. By stacking the lines, a 2D image stream with an indefinite number of lines can be formed. It should be noted that the two approaches are considerably different in terms of hardware construction, image processing implementation and performance.

The key hardware difference between the two approaches is that Step 65B employs additional electronics to derive a perfectly synchronized sampling clock from the laser pulse signals. This ensures the samples (pixels) received by the FPGA are always consistently aligned with the SOL in each line, resulting in 2D image streams with zero distortions between lines. This is particularly important in maintaining image quality and accuracy that is comparable to use of the high-sampling-rate oscilloscope (Step 65A). Another difference is that image processing using Step 65B can be done on-the-fly with a continuous data flow path from FPGA to CPU/GPU. It allows real-time display of the imaging result to users and high-speed data storage without dead time. Hence, Step 65B is particularly useful when real-time data observation, analysis and fine-tuning are essential. On the other hand, use of an oscilloscope (Step 65A) trades the practicality and efficiency with higher maximum analog bandwidth and sampling rate for improved image quality. In this approach, the image data must first be transferred and processed offline on separate computing hardware for visualization and analysis. The specifications and components required for image acquisition for both approaches are summarized in Table 1.

Table 1 | Specifications and components for image acquisition

Approach	High-bandwidth oscilloscope (Step 65A)	Custom FPGA platform (Step 65B)
Main data acquisition hardware	Keysight (DSOX91604A) or Lecroy (SDA 820Zi-B)	FPGA (Teledyne SP device ADQ7DC-PCIe) Host PC (minimum requirement): • CPU: Intel Core i7 6700K • GPU: Nvidia GTX 1080 • Memory: 32 GB DDR4 • Storage: 3 GB/s write speed (SSDs or hard disk drives in RAID configuration)
Signal synchronization method and hardware	Off-the-shelf photodetector module (Newport, cat. no. 818-BB-21) for laser-to-electrical pulse generation oscilloscope built-in level-trigger	Off-the-shelf clock generation modules: • Pulse delay generator with an on-board photodiode (Aerodiode) • Frequency synthesizer (Valon 5009)
Number of data channels	1–4	1–2
Maximum sampling rate	1–2 channels: 80 GS/s; 3–4 channels: 40 GS/s	1 channel: 10 GS/s; 2 channels: 5 GS/s
Maximum analog bandwidth	16 GHz (Keysight), 20 GHz (Lecroy)	3 GHz
Digitized sample precision	16-bit	14-bit
Maximum continuous data capture length	100 MB per snapshot (1.22 ms of continuous data at 80 G/s)	Unlimited[a]
Data capture dead time	~0.49–0.5 s average dead time between each snapshot (equivalent to 0.1 ms of continuous data/ 4.4 MB of data)	Zero[b]

[a]The practical capture length is constrained by actual storage capacity. One can implement the FPGA-based user-configurable region-of-interest detection for real-time data rate/size reduction.
[b]This is valid as long as region-of-interest detection is configured to maintain average data rate within storage speed.

Expertise needed to implement the protocol

The protocol described here (Fig. 5) requires the involvement of:

- An optical engineer who has prior experience in building, modifying and controlling optical instruments, particularly light microscopes. Basic knowledge in hardware electronics control and automation is preferred
- A software engineer with experience in C++, Python and MATLAB
- An experienced microscopist equipped with practical skillsets of biological sample preparation (e.g., cell culture, fluorescence labeling, etc.) and operation of advanced light microscopes

Materials

Biological materials

- Sample to be imaged. In the typical results we show here, we used wild-type (females or males, >2 months old, Jackson Laboratories, Black 6, stock no. 000664) mice for 2D in vivo two-photon fluorescence imaging and *Scenedesmus* (Carolina, 152510) and two cultured breast cell cell lines, MDA-MB231 (ATCC, HTB-26; RRID: CVCL_0062) and MCF7 (ATCC, HTB-22; RRID: CVCL_0031) for 1D flow imaging **! CAUTION** Any lines used should be regularly checked to ensure they are authentic and are not infected with mycoplasma. **! CAUTION** Any experiments involving live animals must conform to relevant institutional and national regulations. All animal experiments were conducted in this procedure according to the National Institutes of Health guidelines for animal research. Procedures and protocols on mice were approved by the Institutional Animal Care and Use Committee at Janelia Research Campus, Howard Hughes Medical Institute.

Reagents

For 1D flow imaging of MCF-7 and MDA-MB231

- For cell culturing medium: RPMI 1640 medium, ATCC modification (Gibco, cat. no. A1049101) for MDA-MB231; and DMEM medium, high glucose, pyruvate (Gibco, cat. no. 11995065) for MCF7
- For cell culturing medium: fetal bovine serum (Gibco, cat. no. 26140079)
- For cell culturing medium: 100× antibiotic–antimycotic (Gibco, cat. no. 15240062)
- For buffer solution: phosphate-buffered saline (PBS) tablets (Invitrogen, cat. no. 18912014)
- Trypsin-EDTA, 0.25% (Gibco, cat. no. 25200072)

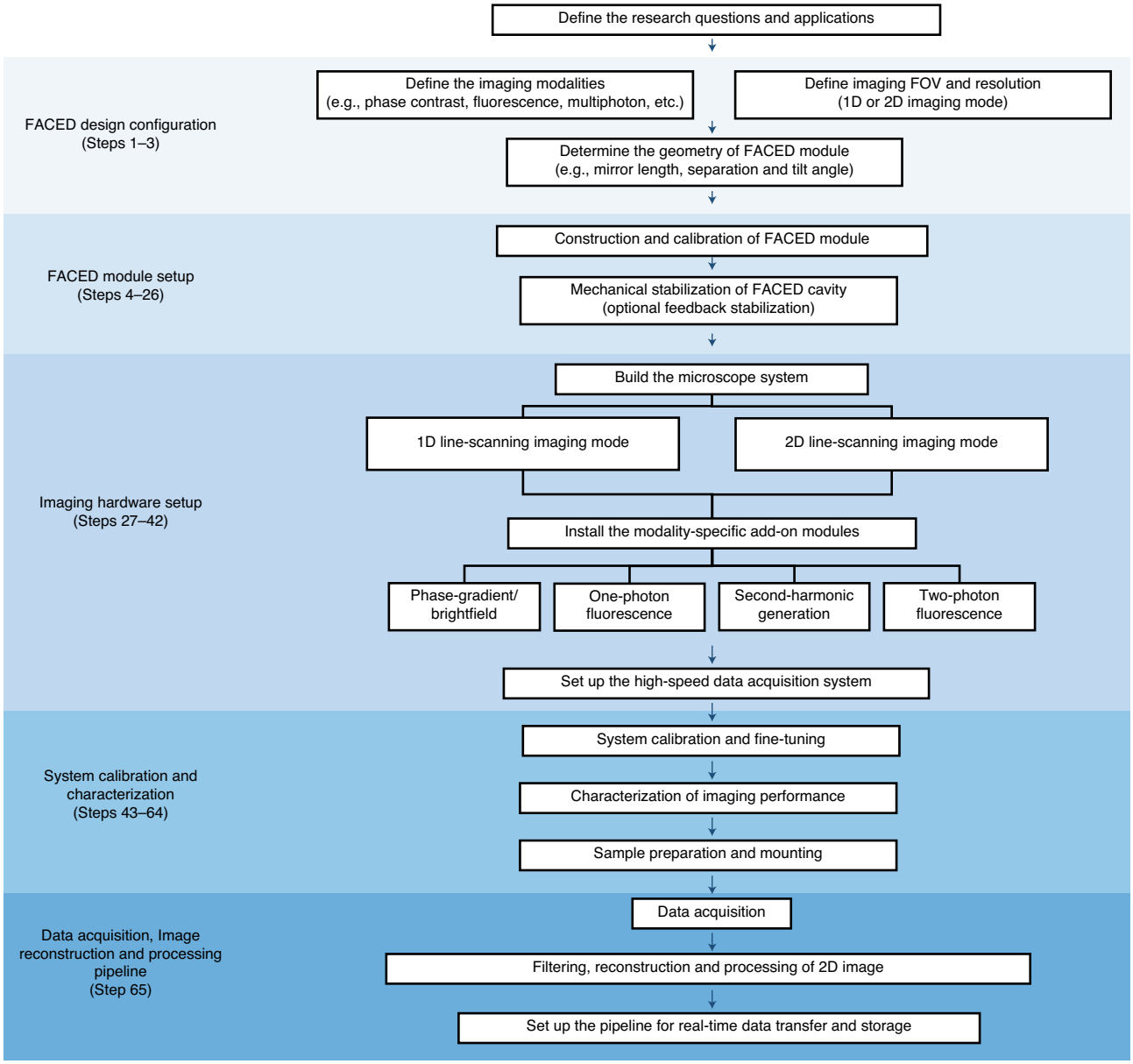

Fig. 5 | General workflow of the protocol. There are five main stages: FACED design configuration; FACED module setup; imaging hardware setup; system calibration and characterization; and data acquisition, image reconstruction and processing.

- For fluorescence dye: Vybrant DyeCycle orange stain (Invitrogen, cat. no. V35005)
- 0.22 μm polyethersulfone filter (Millipore, cat. no. SLGP033RB)

For 1D flow imaging of *Scenedesmus*

- BG-11 medium (UTEX Culture)
- BG-11(-N) medium (UTEX Culture)

For fabrication of microfluidic channel

- Premade custom design silicon wafer mold (custom made) (Supplementary Fig. 1)
- PDMS precursor and curing agent (Dow Corning, SYLGARD 184 Silicone Elastomer kit)
- Custom-made acrylic block
- Biopsy punch, Miltex (Integra LifeSciences, cat. no. 33-31 AA)
- Oxygen plasma machine (Harrick Plasma, cat. no. PDC-002)
- Glass coverslips, 24 × 60 mm, 0.17 mm thickness (ISOLab, cat. no. 075.01.007)
- Plastic tubing (Scientific Commodities, cat. no. BB31695-PE/2)

For system calibration and characterization

- Multifrequency grid distortion target, 76.2 × 25.4 mm (Thorlabs, cat. no. R1L3S3P)
- 2" × 2" positive, 1951 USAF resolution target (Edmund Optics, cat. no. 38-257)
- Fluorescent Nile Red particles, 0.5 μm (mean size), 1.0% wt/vol (Spherotech, cat. no. FP-0556-2)
- ProLong Diamond Antifade mountant (Invitrogen, cat. no. P36965)
- Mini PAP Pen (Thermo Fisher Scientific, cat. no. 008877)
- Glass coverslips, 24 × 60 mm, 0.17 mm thickness (ISOLab, cat. no. 075.01.007)
- Microscope slides, 76 × 26 mm, 1 mm thickness (ISOLab, cat. no. 075.02.005)

Equipment

532 nm pulsed laser for bright-field/phase-gradient and one-photon fluorescence imaging

- 1,064 nm pulsed laser (Time-bandwidth Product, 20 MHz, 500 mW)
- PPLN crystal with oven and mount adapter with 35% conversion efficiency (Covesion, cat. nos. MSHG1064-1.0-1, PV10, OC2, PVP1)
- Pair of C-coated plano-convex lens (Thorlabs, cat. nos. LA1027-C and LA1608-C)
- 1,064 nm, mounted zero-order half-wave plate (Thorlabs, cat. no. WPHSM05-1064)
- 1-axis linear translation stage (Thorlabs, cat. no. XR25P)
- Optomechanics for mounting the optics (Thorlabs)

Laser for SHG imaging

- 710 nm pulsed laser (Spectra Physics, Mai Tai BB, 80 MHz, 1.3 W @710 nm)

Laser for 2PFM imaging

- 920 nm pulsed laser (1 MHz, maximum average power 2 W, pulse width < 100 fs) (laser output from a laser system consisting of a fiber laser (Monaco 1035-40-40, Coherent) followed by an optical parametric amplifier (Opera-F, Coherent))

Beam shaping (optional)

- Mounted high-power precision pinhole (Thorlabs). The pinhole size should be selected based on the input beam diameter and the focal length of the previous lens for beam focusing
- A-coated plano-convex lenses (Thorlabs). The focal lengths should be selected based on the optical system design

Beam expander

- A pair of spherical lenses (focal length depends on laser beam width and the design configuration) (f = 50 mm and 250 mm, Thorlabs, cat. nos. AC254-050-B-ML and AC254-250-B-ML) mounted on a translation stage or 2× beam expander (Thorlabs, cat. no. BE02M-B)

FACED module

- A pair of high-reflectivity mirrors, 200 × 25 × 12.5 mm (FM1, FM2, >99.5% custom made dielectric mirror ios Optics; for 2PFM that employs ultrafast pulses, a pair of high-reflectivity mirrors (>99.9%) with low GDD are used (GDD < 10 fs^2 per reflection at 920 nm, fused silica substrate, 250 mm long and 20 mm wide, Layertec GmbH)
- FACED mirror mounting optomechanics (one is mounted on XY linear translation stage (Thorlabs, cat. no. XYT1) and worm-driven rotation stage (Thorlabs, CR1); one is mounted on a custom-made mirror mounting platform with piezo actuator (POLARIS-P20) for pitch tunning or a Polaris standard kinematic platform (Thorlabs, cat. no. K1M4))
- Open-loop piezo controller (Thorlabs, cat. no. MDT694B)
- Half-wave plate for tuning the polarizing state of the input beam (WP1, mounted zero-order half wave plate for 532 nm/600–900 nm, Thorlabs, cat. no. WPH05M-532/AWPH05M-600, on rotation mount, Thorlabs, RSP1)
- Quarter-wave plate for tuning the polarization state of the reflected beam from the FACED mirror pair (WP2, mounted zero-order quarter waveplate for 532 nm/600–900 nm, Thorlabs, cat. no. WPH05M-532/AWPH05M-600, on a rotation mount, Thorlabs, RSP1)
- Polarizing beamsplitter (BP1, Thorlabs, cat. no. PBS101/PBS102, mounted on a kinematic platform, cat. no. KM100M, by a clamping arm, cat. no. PM3)
- A-coat cylindrical lens (CL1, Thorlabs, focal length should be selected on the basis of the optical system design, cat. no. LJ1267RM-A, f = 250 mm for fluorescence setup; cat. no. LJ1695RM-B, f = 50 mm for SHG imaging setup/for 2PFM setup)

- Cylindrical lens mounting optomechanics (linear translation mount and rotation mount, Thorlabs, cat. nos. LRM1 and CXY1)
- Adjustable slit for adjusting the incident beam width (A1; Thorlabs, cat. no. VA100)
- Adjustable slit for blocking the peripherical light modes (A2; Thorlabs, cat. no. VA100)

Stabilization module
- Quadrant photodiode (QPD; First Sensor, cat. no.718-QP5.8-6-TO5)
- Micro-controller unit (ST Microelectronics Discovery, cat. no. F407)
- Home-made printed circuit board for signal conditioning
- A-coat plano-convex lens (L6, focal length should be selected based on the optical system design, Thorlabs)
- Nonpolarizing beamsplitter (BS1, splitting ratio should be selected based on power budget, Thorlabs)

Relay optics for 1D flow imaging (setup (I) and (II))
- Spherical lens for projecting the virtual sources on conjugate plane CP1 (L2; Thorlabs, f = 150 mm, cat. no. LA1433-B, for 710 nm)
- Spherical lens for magnifying/demagnifying the virtual sources (L3 and L4; Thorlabs, L3: 100 mm, cat. no. LA1509-B, L4: cat. no. LA1509-B for 710 nm setup)
- Halfwave plate for tuning the SHG signal strength (Thorlabs, cat. no. AQWP05M-600, with RSP1)
- Tube lens (TL; Thorlabs, LA1433-B)
- Optomechanics for holding the lens and waveplates—lens mount, rotation mount, post and postholders (Thorlabs, cat. nos. LMR1, RSP1, PH1/1.5/2/3, TR1/1.5/2/3)

Relay optics for 2D raster scanning imaging (setup (III))
- 4-f system to relay the pupil plane (i.e., the focal plane of the cylindrical lens) of the FACED laser scanner to the midpoint of a pair of closely and orthogonally arranged *x*- and *y*-galvo mirrors: a pair of achromatic doublets (L2 and L3; Thorlabs, cat. nos. AC508-500-B and AC508-250-B)
- *x*-*y* galvo mirrors (Cambridge Technology, cat. no. GM-6215 H) with servo driver (Cambridge Technology, cat. no. 673) and controller (Cambridge Technology, ScanMaster Controller)
- Adjustable slit for defining the FOV of the slow axis (A3; Thorlabs, cat. no. VA100)
- Scan lens (L4; Thorlabs, cat. no. SL50-2P2)
- Tube lens (TL; Thorlabs, cat. no. TTL200MP)

Alignment inspection module (only for setup (I) and (II) in Fig. 5)
- Pellicle beam splitter mounted on a flipper (BS2, cat. nos. BP108 with BP107)
- Focusing spherical lens (L5; Thorlabs, cat. no. AC254-150-B-ML)
- Camera (CAM; Thorlabs, cat. no. DCC1645C)

Vertical mounted imaging setup and addition detection module for the bright-field/phase-gradient and fluorescence imaging setup (I)
- Dichroic mirror (DM1; Semrock, cat. no. FF552-Di02-25x36)
- Illumination and detection objectives (OBJ1, 40×, 0.6 NA, 2.6–2.8 WD, Nikon, cat. no. MRH08430; OBJ2, 40×, 0.8 NA, 3.5 WD, Nikon, cat. no. MRD07420)
- 10 GHz, 320–900 nm ultrafast photodetector (ALPHALAS, cat. no. UPD-30-VSG-P)
- 10 GHz linear amplifier (Tektronix, cat. no. PSPL5866)
- A-coat plano-convex lens for focusing the signal on the photodetector and PMT1 (L7, L8, L9; Thorlabs, focal length should be selected based on the optical system design)
- Band pass filter for detecting orange fluorescent signal (BF1; Semrock, FF01-575/15-25)
- Photodetection modules for single fluorescence imaging (PMT1; Hamamatsu, H10721-20-02)
- Amplifier and power supply for PMT1 (Hamamatsu, C10709)
- Knife edge (K)

Vertically mounted imaging setup and addition detection module for the bright field imaging and SHG setup (II)
- Dichroic mirror (DM2; Semrock, cat. no. FF660-Di02-25x36)
- Illumination and detection objectives for brightfield and SHG setup (OBJ1, 40×, 0.75 NA, FWD 0.71 mm, Carl Zeiss, Objective EC 'Plan-Neofluor' 40×/0.75 M27; OBJ2, condenser lens, cat. no. ACL25416U-B)
- Two-axis translation mount for objectives

- Ultrafast and high-bandwidth photodetector for bright-field images (PD1; Amplified GaAs Photodetector, EOT Optics, cat. no. ET-4000A)
- Dichroic mirror (DM2; Semrock, cat. no. FF552-Di02-25x36)
- Band pass filter for SHG signal (BF2; Thorlabs, cat. no. FL355-10)
- Band pass filter for SHG signal (BF2; Semrock, cat. no. F01-405/150-25)
- Spherical lens for focusing the signal on the PMT2 (L10; Thorlabs, cat. no. LA1805-A-ML) (focal length should be selected based on the optical system design)
- Photodetection modules for detecting SHG signal, hybrid photodetector (PMT2; hybrid photodetector, cat. no. R10467U-40) with an amplifier (Hamamatsu, cat. no. C11178) and power supply (Hamamatsu, cat. no. C12929)

Vertically mounted imaging setup and addition detection module for the 2PFM setup (III)

- Dichroic mirror (DM1; Semrock, cat. no. FF665-Di02-25X36)
- Bandpass filter for fluorescence emission (BF1; Semrock, cat. no. FF01-680/SP)
- One objective for both illumination and detection in two-photon fluorescence in vivo imaging (OBJ1; Olympus, 25×/1.05 NA, cat. no. XLPLN25XWMP2)
- Piezo stage to axially move the objective lens (Physik Instrumente, cat. no. P-725K094)
- PMT with the current protection circuit removed (Hamamatsu, cat. no. H7422P-40 MOD)

Common optics for the imaging setups

- Optomechanic assembly for mounting the dichroic mirror—a Kinematic Cage Cube Platform (cat. no. B4C) in a standard 30 mm cage (cat. no. C6W) with an adaptor for holding rectangular optics (Thorlabs, cat. no. FFM1) and a cover plate (Thorlabs, cat. no. B1C)
- Optomechanic assembly for mounting the imaging part in vertical direction—1.5 inch post with (Thorlabs, cat. no. DP14A) mounting clamp (cat. no. C1511) and linear translation stage (Thorlabs, cat. no. LX10); cage rods (Thorlabs, cat. nos. ER1, ER2) and lens tube (Thorlabs, cat. nos. SM1L03, SM1L05, SM1L10, SM1V05, SM1V10) for blocking the light between the dichroic mirror, bandpass filter, collecting lens and PMT and connecting them; post and post holders for supporting the optomechanic assembly (Thorlabs, cat. nos. TR1, PH082E, CF125)

Sample stage for 1D flow imaging

- XYZ linear stage (Newport, cat. no. M-562-XYZ), with one manual actuators (Newport, cat. no. SM-13 for *x*-axis, and two motorized actuators cat. no. LTA-HS for *y*-axis and cat. no. DM-25 for *z*-axis)
- Controller for motorized actuator (Newport, cat. no. ESP301)
- An assembly of optomechanical components (Thorlabs, cat. nos. POLARIS-K1M4/M, PLS-P1, POLARIS-CA1) mounted on the XYZ linear stage to hold the microscope slide holder (Thorlabs, cat. no. MAX3SLH)
- Syringe pump (Longerpump, cat. no. LSP01-1BH)

Sample stage for mouse

- 3D translation stage to hold the mice (Dover, cat. nos. XYRB-1010 and ZE-10)

Data acquisition and processing system

- High-speed digitizer (National Instruments, sampling rate: 625 MS/s, 2G onboard memory, cat. no. PXIe-5160; Keysight, cat. no. DSOX91604A, sampling rate 80 GS/s for two channels; or Lecroy, sampling rate 80 GS/s for two channels)
- Customizable FPGA board (SP Devices, cat. no. ADQ7DC-PCIE)
- Host PC linked with FPGA (with two or more Gen3 PCIe ×16 physical dimension slots for the ADQ7 digitizer card and GPU adapter; a CPU with at least four physical cores; with M.2 NVMe solid-state drive (SSD) storage capable of at least 3 GB/s sequential write speed)
- FPGA Design tools (Xilinx Vivado 2017.1 with full license support of Kintex UltraScale (xcku085) and all its on-chip IP peripheral)
- ADQ7 FPGA development kit (Revision 53589 for ADQ7DC PCIe)
- Teledyne SP Devices Software Development Kit (Device driver and API Revision r53490)

Reagent setup

Cell culturing medium for MDA-MB231

Add 10% fetal bovine serum (Gibco, cat. no. 26140079) and 1% antibiotic–antimycotic (100×, Gibco, cat. no. 15240062) to the RPMI 1640 medium (ATCC modification, Gibco, cat. no. A1049101), then store in 4 °C. The medium needs to be used within 1 month.

Cell culturing medium for MCF7

Add 10% fetal bovine serum (Gibco, cat. no, 26140079) and 1% antibiotic–antimycotic (100×, Gibco, cat. no. 15240062) to the DMEM media (high glucose, pyruvate, Gibco, cat. no. 11995065), then store in 4 °C. The medium needs to be used within 1 month.

Cultured cell line, breast cancer cell (MDA-MB231, MCF7)

Culture the cell line in an incubator with 5% CO_2 under 37 °C.

PBS

Dissolve a PBS tablet in 500 mL of distilled water to prepare the 1× PBS. After the tablet is fully dissolved, sterile filter the solution by using 0.22 μm polyethersulfone filter (Millipore, cat. no. SLGP033RB). The solution can be stored at 15–30 °C and should be used within 1 year.

Procedure

Designing the targeted FACED imaging modalities ● Timing 3–4 d

▲ **CRITICAL** In this procedure, we describe the three FACED imaging configurations: bright-field/phase-gradient, one-/two-photon fluorescence and SHG imaging. In principle, the optimal specifications of the FACED module are imaging modality dependent. Therefore, if multimodal configuration is needed, special attention should be paid to the potential tradeoff among different imaging performance metrics, e.g., FOV, spatial resolution and temporal resolution.

1 Define the targeted imaging modality and decide whether multimodality (such as fluorescence imaging combined with bright-field imaging or SHG imaging combined with bright-field imaging) is required.

2 Define the targeted imaging spatial resolution, FOV (particularly along the fast axis), and temporal resolution (temporal separation between adjacent virtual source, or the effective 'dwell time' of each scanning focal spot. The design rationale is described in 'Experimental design'.

3 Determine the major design specifications of the FACED module. They include the misaligned angle of the mirror pair (α), the mirror-pair separation (S), the length of the mirrors (L) and the input light beam condition (refer to the design theory in Box 1).
▲ **CRITICAL STEP** The design process can be iterated between Steps 2 and 3 until the best optimal targeted specifications are identified.

FACED module setup and calibration ● Timing 14 d

▲ **CRITICAL** The procedure for the implementation of the FACED module (Steps 4–26) is broadly applicable to many FACED microscopy modalities and, thus, different choices of pulsed laser sources. In general, we suggest using the pulsed laser source with a pulse width of subpicosecond to picoseconds and a repetition rate of 1 MHz or above. In the case of multiphoton imaging, a standard pulse compressor for dispersion compensation (preferably with the GDD > 10,000 fs^2) is needed after the laser system[42]. Standard specifications and setup are detailed elsewhere[43]. The specific details of the laser specification depend on the targeted applications (see 'Spatiotemporal resolution of the FACED microscope').

▲ **CRITICAL** In this procedure, we describe how to install the entire system on an optical table with vibration isolation supports. For the sake of system compactness, it is also feasible to mount the setup on any mechanically stable platform. In this case, active feedback control for antivibration is likely to be important.

4 Set up the laser source on the optical table. Turn on the laser source. Note that general pulse picking steps might be needed (e.g., by using AOD) if the repetition rate does not match the targeted line-scan rate of the application. Detailed design considerations are detailed in 'Spatiotemporal resolution of the FACED microscope'.

5 Align the two-lens beam expander (either the Keplerian or Galilean telescope) (Fig. 6) to magnify or diminish the collimated beam size for matching the design parameters of the FACED module

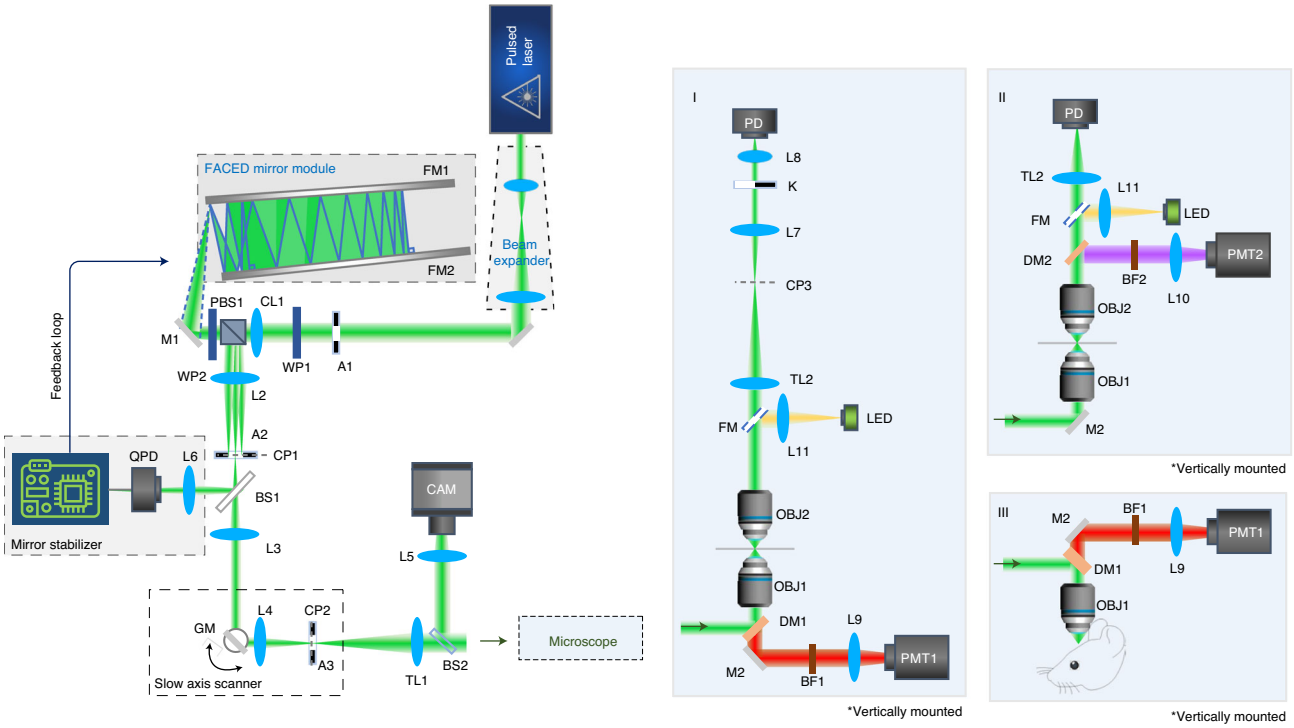

Fig. 6 | Schematics of the FACED imaging system of three different implementations (I) (II) and (III). *Not to scale. FACED mirror pair: FM1, FM2; adjustable slit: A1, A2, A3; waveplate: WP1, WP2; cylindrical lens: CL1; polarizing beam splitter: PBS; mirror: M1, M2; spherical lens: L1, L2, L3, L4, L5, L6, L7, L8, L9, L10; beam splitter: BS1, BS2; conjugate plane: CP1, CP2, CP3; quadrant photodiode: QPD; galvo-mirror: GM; tube lens: TL1; dichroic mirror: DM1, DM2; bandpass filter: BF1, BF2; photomultiplier: PMT1, PMT2; flipping mirror: FM; knife edge: K; photodiode: PD. For more details, refer to the equipment list.

(in this case, the beam size determines $\Delta\theta$ and, hence, the number of virtual sources N) (Eq. 8). Make sure the laser beam will enter the beam expander in a straight line at its center. An additional adjustable slit (A1) might be required to finely adjust the beam size.

6 Direct the expanded laser beam to the center of the cylindrical lens (CL1) and pass the beam through a half-wave plate (WP1), a polarizing beam splitter (PBS1) and a quarter-wave plate (WP2) (Fig. 6). Again, ensure the beam is aligned at the center of these optical components.

7 Adjust the orientation of WP1 in order to rotate the linear polarization state of the beam until the laser power after PBS1 is at its maximum.

8 Mount the FACED mirror pair on the kinematic mounts, which offers high-resolution angular adjustment and long-term laser-beam alignment stability.

▲CRITICAL STEP Ensure that the kinematic mounts could provide the angular resolution below 50 μrad in both the pitch and yaw adjustments. This is essential for fine-tuning the density of the virtual source arrays (thus, the density of the scan spots), as well as the line-scan beam alignment along the slow axis (Fig. 7).

▲CRITICAL STEP Be aware of the mechanical stress exerted on the FACED mirrors by the kinematic mounts. Excessive stress could result in deformation of the mirror, which in turn distorts the scanning beam profile.

? TROUBLESHOOTING

9 Position one of the FACED mirrors (FM1) on the focal plane of the cylindrical lens CL1. We recommend placing a mirror (M1) between CL1 and the FACED mirror pair for fine-tuning of the incident light angle onto the FACED mirror if the distance between the FM1 and WP2 is sufficient.

10 Adjust the FACED mirror (FM1) such that the focusing beam is normally incident onto the entrance point O, which should be near the edge of the FM1.

11 Fine-tune the yaw rotation of the FACED mirror (FM1) (in the anticlockwise direction in Fig. 7) such that the reflected beam (from O) does not overlap with the original incident beam.

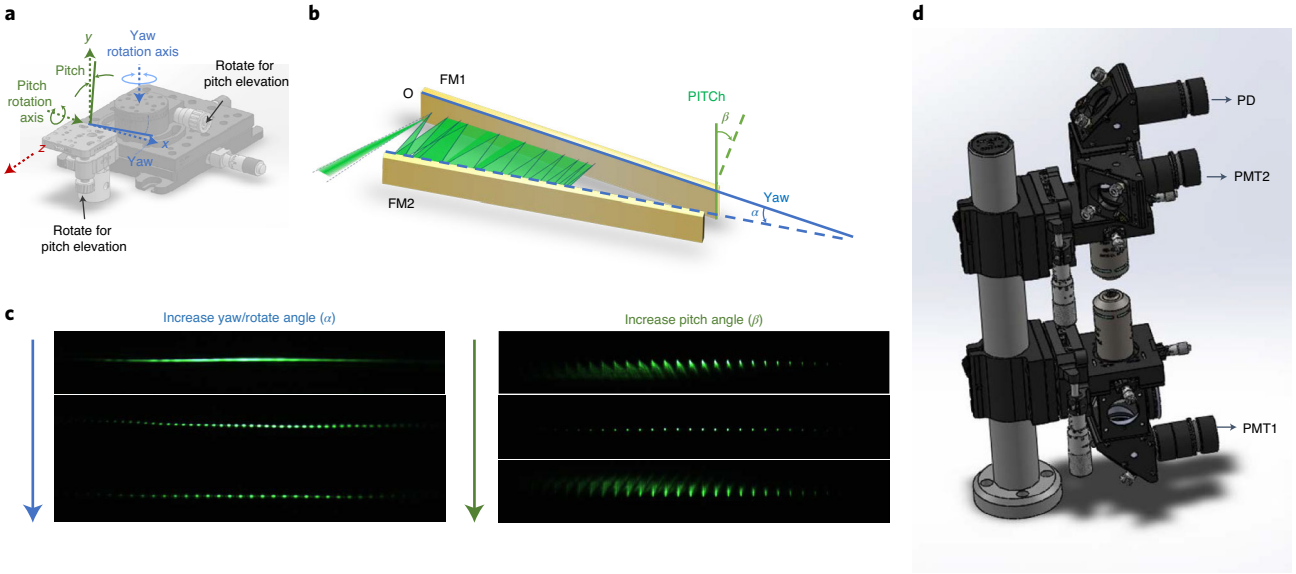

Fig. 7 | Mounting of the FACED mirror pair and vertical imaging part. a, An example assembly of the mounting stage of FACED mirror pair. **b**, Illustration of the yaw and pitch adjustment of the FACED mirror pair. **c**, Effect of tuning the yaw and pitch angles of the mirror pair on the beam scanning profile. **d**, An example assembly of the vertically mounted imaging setup. Images adapted from SolidWorks Models provided compliments of Thorlabs.

12 Position the second mounted FACED mirror (FM2) away from FM1 by the targeted separation (S). Multiple reflections of light between FM1 and FM2 should now be observed.
▲ **CRITICAL STEP** To facilitate the subsequent fine-tuning steps, we advise ensuring the mirror pair are almost parallel along *X*, *Y* (pitch and yaw rotation axis).

13 Adjust the pitch angle of the FACED mirror (FM2) such that the beam height (from the optical table surface) is maintained throughout the multiple reflections upon the mirror pair.

14 Carefully adjust the yaw rotation of the FM2 (i.e., the mirror tilt angle α) to prevent part of the beam from being leaked out from the far end of the mirror pair.
▲ **CRITICAL STEP** Note that this is also a key step to find the 'approximate' condition under which an array of virtual sources is generated. That means the beamlets (split from the incident beam) should be retroreflected back to entrance *O*. Precise tuning of the virtual source number is not necessary for this step.

15 Further adjust the yaw and pitch rotation of both the FM1 and FM2 to (a) maintain the beam height throughout all the multiple reflections between FM1 and FM2 and (b) align and direct the retroreflected beam back to the BS1, which will reroute the beam toward the microscope.
▲ **CRITICAL STEP** Note that this is also a key step to find the 'approximate' condition under which an array of virtual sources is generated. That means the beamlets (split from the incident beam) should be retroreflected back to entrance *O*. Precise tuning of the virtual source number is not necessary for this step.
? TROUBLESHOOTING

16 Adjust the orientation of the WP2 to maximize the power of the returning beam after being rerouted by the BS1.

17 Place a spherical lens (L2) to project the image of the virtual sources onto the conjugate plane CP1 (Figs. 3 and 6), which is approximately at the distance of IL_k after L2.

18 Place a camera or a laser-beam viewing card at the plane CP1 temporarily to visualize and optimize the image quality of the virtual sources (i.e., the array of foci). Additional relay spherical lens might be required to resize the foci to fit the FOV of the camera.

19 Obtain the desired (subset of) virtual sources and optimize the profile of the foci captured by the camera/viewing card by identifying the $k_{start}{}^{th}$ virtual source on the camera. To do this, undertake an iterative tuning of the following three substeps:
- Tune the yaw rotation of the first FACED mirror FM1 to set the targeted incident angle
- Tune the yaw rotation of the second FACED mirror FM2 to maintain the same α. The purpose of this step is to obtain the targeted number of virtual sources *N* that can all be reflected back to the beam splitter BS1 and projected onto the camera plane (CP1)

- Use a lens tissue to cut cross the light between the FACED mirror pair from the far end until there is only one focus spot appearing on the plane CP1 (captured by the camera/viewing card). Check if the position of the tissue paper is approximately at $R(1 - \cos k_{start}\alpha)$ from the edge of FM1

20 Repeat Step 19 until the position of the focus spot is correct. The camera can then be removed after this step.

▲ **CRITICAL STEP** During the iterative tuning process, always ensure the beam height is maintained by adjusting the pitch rotation of both the FACED mirror FM1 and FM2.

▲ **CRITICAL STEP** The angular range of the FACED mirror mount may not be sufficient. In this case, the mirror pair might need to be repositioned and the FM1 and FM2 readjusted, by starting from Step 8 again. Alternatively, the light cone incident angle can be tuned by adjusting the yaw rotation of mirror M1 before being focused at the entrance O of the FACED mirror pair.

21 Place the adjustable slit (A2) at the conjugate plane CP1 to block the residual light and the peripheral virtual sources that might have low intensity or temporally overlap with the next line scan.

22 Verify the temporal profile of the virtual sources projected on the plane CP1 by placing a free-space (large-area) photodiode at the plane CP1. An additional focusing lens might be needed for higher detection efficiency.

▲ **CRITICAL STEP** This step can also be used to check the duty cycle of each line scan in time, especially to verify that there is no temporal overlap between adjacent line scans.

23 Build a simple enclosure (preferably made of acoustic-proof materials) that protects the FACED module from ambient perturbation. If you need to mechanically stabilize the FACED cavity, then proceed to the next step; otherwise, proceed directly to Step 27.

▲ **CRITICAL STEP** To facilitate routine calibration of FACED module, add a beam splitter (BS2) (Thorlabs, pellicle beam splitter BP108) and a camera (Thorlabs, cat. no. DCC1645) after the plane CP1, both of which form a monitoring path for characterizing the beam profile of the virtual sources.

Mechanical stabilization of FACED cavity (optional feedback stabilization) ● Timing 3–4 d

▲ **CRITICAL** This section is required only if an additional active feedback module is needed to stabilize the FACED mirror pair (Supplementary Manual 1 and Supplementary Figs. 2–6).

24 Replace the camera with a QPD for detecting misalignment in the beam position in the Fourier plane of the virtual sources (Fig. 6).

25 Project the Fourier plane of the virtual sources onto the center part of the sensor area of the QPD by a spherical lens (L6).

26 Connect the analog electrical output of the QPD to a microcontroller (ST Microelectronics Discovery F407) through a custom signal conditioning board (Supplementary Manual 1), which drives the piezoelectric actuator (Thorlabs, cat. no. POLARIS-P20) of one of the FACED mirror mounts.

▲ **CRITICAL STEP** The QPD is a segmented-quadrant position sensor that consists of four identical quadrant photodiodes. It can measure the 2D position of an incident laser beam by quantifying the detected photocurrent at each sector (Supplementary Manual 1). It is essential to first calibrate the center position of the QPD prior to the actual measurement.

Building the microscope system ● Timing 7–8 d

▲ **CRITICAL** This section describes the procedures for implementing the illumination for the two imaging modes compatible with FACED microscopy: (A) 1D (static) line-scanning mode or (B) 2D full-frame mode. The main difference between the two operations is the additional beam scanning module that provides slow-axis scan orthogonal to the FACED line scan (i.e., fast axis).

27 Follow option A to implement illumination for 1D (static) line-scanning mode or option B for 2D full-frame mode.

▲ **CRITICAL STEP** The key purpose is to project the line-scan profile on the imaging plane with the desired FOV and foci density. Basic alignment of the illumination path requires at least one module of telecentric lenses (L3 and L4) to conjugate the image of the virtual source array to the back focal plane of the TL, as well as to the front focal (imaging) plane of the objective lens (OBJ).

(A) **1D line scanning imaging setup**

(i) Add the telescopic lenses (L3 and L4) along the beam path, and locate the image profile of the virtual source array in the front focal plane of L4.

(ii) Align the tube lens (TL1) and the microscope objective lens (OBJ1) such that the virtual source array is finally conjugated onto the front focal plane (image plane) of OBJ1.

▲ **CRITICAL STEP** Additional telescopic module might be needed between L4 and TL1 to further adjust the overall beam size and the FOV, with the overall magnification (from CP1 to the image plane of OBJ1) of $M = (f_3/f_2)\cdot(f_{TL}/f_4))\ M_{extra}$, where M_{extra} is the magnification of the extra telescopic module.

▲ **CRITICAL STEP** The configuration of the imaging module is similar to an inverted light microscope, in which the illumination of the scanning foci (virtual sources) is launched upward through the objective lens (OBJ1). This can be done by adding a right-angled dichroic mirror (DM1) to direct the beam upward through the microscope. The overall beam profile should be aligned at the center of the right-angle mirror. The dichroic mirror (DM1) reflects the illumination beam and transmits the epifluorescence (one-/two-photon fluorescence) emission.

(iii) Place a plane mirror on the imaging plane (and adjust its tilt angle and axial position away from OBJ1) to locate the image of the scanning foci reflected from this mirror onto another conjugate plane. This requires an additional pellicle beamsplitter (BS2) mounted on a flipper mount right before OBJ1, such that the back-reflected beam is routed to a focusing lens (L5) and a camera (CAM) (Fig. 6). This helps monitor the profile of the scanning foci on the imaging plane (i.e., front focal plane of OBJ1) and align the BS2 and CAM. The mirror is then removed after this step.

(iv) Assemble the sample stage, and place a glass coverslip on the sample stage to reflect scanning foci profile onto the camera (CAM) and also transmit the profile through the second objective lens (OBJ2). Fine-tune the axial translation, and adjust tilting of the sample stage and camera to obtain the sharpest image of the scanning foci.

(v) Align the second objective lens (OBJ2). Fine-tune the axial translation of the OBJ2 so that the beamlets transmitted through OBJ2 are collimated along the slow axis.

(vi) Add another light path for aligning the sample stage to the targeted imaging plane by undertaking the following substeps:

- Add a flipper mirror (FM) along the transmitted light path after OBJ2
- Align a LED source (with an optional diffuser in front of the LED) and a condenser lens (L6) together, which deliver the LED illumination on the sample plane (through OBJ2)
- Place a patterned test sample on the sample stage (e.g., a resolution target), and adjust axial translation of the sample stage to bring the image of the test sample in sharp focus on the camera (CAM)
- Unflip FM after the alignment. This alignment step is required before each imaging experiment

▲ **CRITICAL STEP** This step ensures the sample plane coincides with the scanning foci plane.

▲ **CRITICAL STEP** Steps (iv)–(v) can provide additional assistance for tuning the focus in the imaging system, including the 1D flow imaging system for (I) bright-field/phase contrast and fluorescence and (II) bright-field and SHG imaging contrast.

(B) **2D raster scanning imaging setup**

(i) Place a spherical lens (L3) such that CP1 is the front focal plane of L3.

(ii) Place the GM scanning system (Cambridge Technology, cat. no. GM-6215 H) on its Fourier plane of CP1 through the lens L3 (Fig. 6). Turn on the GM scanning system, and make sure that the line beam is at the center (pivot) of the GM.

(iii) Place another spherical lens (L4) such that it relays the virtual source images from CP1 to the back focal plane of L4 (CP2). If required, also place an adjustable slit (A3) on this plane (CP2). This slit can be used to define the FOV along the slow axis of the final image.

▲ **CRITICAL STEP** Note that the FOV along the slow axis is defined as $FOV_y = f_4 \tan(\gamma) f_{obj}/f_{TL}$ where γ is the total scanning angle of the slow-axis scanning system, which is governed by scanning angular range of the GM and/or the size of the S2 (Fig. 6).

(iv) Align the tube lens (TL1) and the microscope objective lens (OBJ1) such that the virtual source array is finally conjugated onto the front focal plane (image plane) of OBJ1.

(v) Place a plane mirror on the imaging plane of OBJ1 (and adjust its tilt angle and axial position from the OBJ1) to locate the image of the scanning foci reflected from the mirror onto another conjugate plane. This requires an additional pellicle beamsplitter (BS2) mounted on a flipper mount right before OBJ1 such that the back-reflected beam is routed to a focusing lens (L5) and a camera (CAM) (Fig. 6). This helps monitor the profile of the scanning foci on the imaging plane (i.e., front focal plane of OBJ1) and align the BS2 and CAM.

(vi) Turn on the GM scanning system. Monitor the actual scanning range using the camera (CAM) as described in the CRITICAL Step 27A(iii). Fine-tune the scanning FOV along the slow axis, and also iteratively adjust the positions of the GM such that the beam profile does not wobble when inspected at the camera (CAM).

(vii) Fine-tune the aperture size of the adjustable slit (A3) to block any spurious light at the edges of the scanning FOV.

(viii) Remove the mirror mounted in Step (v). Assemble the sample stage, and place a glass coverslip on the sample stage to reflect scanning foci profile onto the camera (CAM). Fine-tune the axial translation of the sample stage and camera to obtain the sharpest image of the scanning foci. Note that setup (III) for 2PFM of the mouse brain requires additional steps to optimize the imaging focus (see Step 64B) and thus to make sure the sample plane coincides with the scanning foci plane.

(ix) (Optional) Repeat Step 27A(v)–(vi) for further system calibration in the transmission mode. Once the calibration is done, remove OBJ2 and the path after it to leave room for in vivo mouse brain imaging using 2PFM.

Installing the modality-specific add-on modules ● Timing 1 d

▲ **CRITICAL** Regardless of the imaging contrasts, the detection path should be built in a cage system enclosed with the lens tube assemblies to provide ambient light shielding. Additionally, the specimen stage assembly and the photodetector module (e.g., PMT and HPD) should also be secured within the light-proof enclosure.

28 Set up the detection systems required for the imaging contrasts by following option (A) for bright-field or phase gradient contrast; option (B) for one-/two-photon fluorescence contrast; and/or option (C) for SHG contrast.

▲ **CRITICAL STEP** The imaging setup can comprise any one of or all these imaging contrasts, and choice is dependent on the research question being addressed.

(A) **Bright-field or phase gradient image contrast**

(i) Position and align tube lens (TL2) after the objective lens (OBJ2) to bring the scanning foci profile to the conjugate plane CP3.

(ii) Add the telescopic lenses (L7, L8) to further conjugate the scanning foci onto the high-speed photodiode (PD) (model UPD-30-VSG-P, ALPHALAS). The magnification of the telescopic lenses should be set to match the size of the detected beam profile with the sensor area.

(iii) Mount the PD on a three-axis-translation stage, and connect it with the oscilloscope or the custom FPGA platform through an SMA cable (see Steps 29–42 for the setup).

! **CAUTION** An electrostatic discharge wrist strap should be used before handling the photodiode and oscilloscope to prevent electrostatic damage to the equipment.

(iv) Position a knife edge (K) at the common focal plane of L7 and L8 (i.e., Fourier plane of CP3). The knife edge could be oriented to partially block the beam in either the horizontal or vertical directions. Add a linear translation stage if fine adjustment of the position of the partial beam block is required. This knife-edge step essentially produces the phase-gradient (differential-interference-contrast-like) contrast based on a concept similar to Schlieren photography[44]. The orientation of the shadowing effecting follows that of the beam block by the knife edge[45].

(B) **One-/two-photon fluorescence image contrast**

▲ **CRITICAL** The detection light path for both one- and two-photon fluorescence imaging share the same configuration, except the specifications of the dichroic mirrors and PMTs. The overall setup procedures follow the standard practice of assembling the (epifluorescence) detection path of a fluorescence light microscope[1].

(i) Adjust the rotation of the mirror M2, which is placed in the cage mount connected to the dichroic mirror (DM1), to align the fluorescent beam at the center of the cage mount aperture.

(ii) Add a bandpass filter (BF1), which further rejects the residual excitation light, after M2. Extend the cage system from M2 by adding a lens tube, which shields the light path.

(iii) Add a collector lens (L9) after BP1, and place a PMT (PMT1) at the focal plane of L9. Note that the choice of the focal length of L9 depends on the NA and sensor area of PMT1.

(iv) Place a fluorescent sample on the sample stage. Note that the sample should produce strong fluorescent emission (e.g., a piece of fluorescently dyed lens tissue fixed on a glass slide, or a cuvette filled with fluorescent solution). Fine-tune the mirror M2 and the collector lens L9 to align the fluorescent light to PMT1. Cover the light path between PMT1 and L9 with another lens tube.

? TROUBLESHOOTING

(v) Turn on the power supply of PMT1. Connect PMT1 to an electronic amplifier (with an electronic SMA cable) and then an oscilloscope.

! CAUTION Make sure to set PMT voltage within the range recommended by the manufacturer's specifications.

(vi) Check the signal displayed on the oscilloscope, and fine-tune the position of PMT1 to maximize the detected fluorescence signal.

(C) **SHG image contrast**

▲ CRITICAL A SHG microscope is typically configured either in forward or backward collection mode, depending on the structures of the specimens[46]. In this protocol, we focus on the forward collection mode, which has the same configuration as the backward mode. For backward collection configuration, follow the setup steps described in Step 28B.

(i) Add a combination of two wave plates (zeroth-order half-wave plate $\lambda/2$ and quarter-wave plate $\lambda/4$) before DM1 to achieve circular polarization at the imaging plane after OBJ1. Note that circular polarization is preferred in non-polarization-resolved SHG imaging. Otherwise, SHG excitation with linear polarization should be used.

(ii) Add a dichroic mirror DM2, which is placed in the cage mount connected to the objective (OBJ2).

(iii) Add a bandpass filter (BP2), which further rejects the residual excitation light, after DM2. Extend the cage system from DM2 by adding a lens tube, which shields the light path.

(iv) Add a focusing lens L10 after DM2. The separation between L10 and OBJ2 is approximately set as the sum of the focal lengths of L10 and OBJ2.

(v) Place a PMT or HPD (PMT2) roughly at the focal plane of L10.

▲ CRITICAL STEP In the forward SHG collection mode, it is sometimes more favorable to use the second objective lens (OBJ2) with a higher NA than OBJ1 to more efficiently collect the forward dual-lobed SHG emission pattern (Fig. 6). Hence, the forward collection mode does not follow classical Kohler geometry. This implies that the light transmitted through OBJ1 would not be collimated. Hence, the positions of both lens L10 and PMT2 should further be fine-tuned later to maximize the SHG signal collection efficiency. An additional telescope might be required to further reduce the beam size to match the sensor area of the HPD. For high-speed SHG imaging, HPD could be more favorable than traditional PMT because of the superior combination of high temporal resolution and high sensitivity.

! CAUTION An electrostatic discharge wrist strap should be used before handling the photodiode and oscilloscope to prevent electrostatic damage to the equipment.

Setup of high-speed data acquisition system ● Timing 15 d

▲ CRITICAL Two different approaches for data acquisition and processing are described in this protocol: (1) using a high-bandwidth real-time oscilloscope and (2) using a custom FPGA platform with GPU computing support. In the initial stage of the system setup, we recommend using the oscilloscope first to perform optical alignment of the system, and calibration of the imaging performance. Once these initial steps are done, one can then switch to the FPGA/GPU platform for real-time image acquisition routines.

Oscilloscope setup ● Timing 1 d

▲ CRITICAL The following steps are to set up the oscilloscope for optimizing the optical alignment of the system as well as characterizing the general imaging performance.

29 Connect the photodetectors (i.e., PD, PMT1 and/or PMT2) to the digitizer of the oscilloscope.

30 Use a beamsplitter (BS_T) to split a small fraction of the laser beam from the laser source (1% in optical power) and align this beam to a photodetector (PD_T), which generates a trigger reference signal fed to the oscilloscope (Fig. 8) for synchronized line-scan image acquisition.

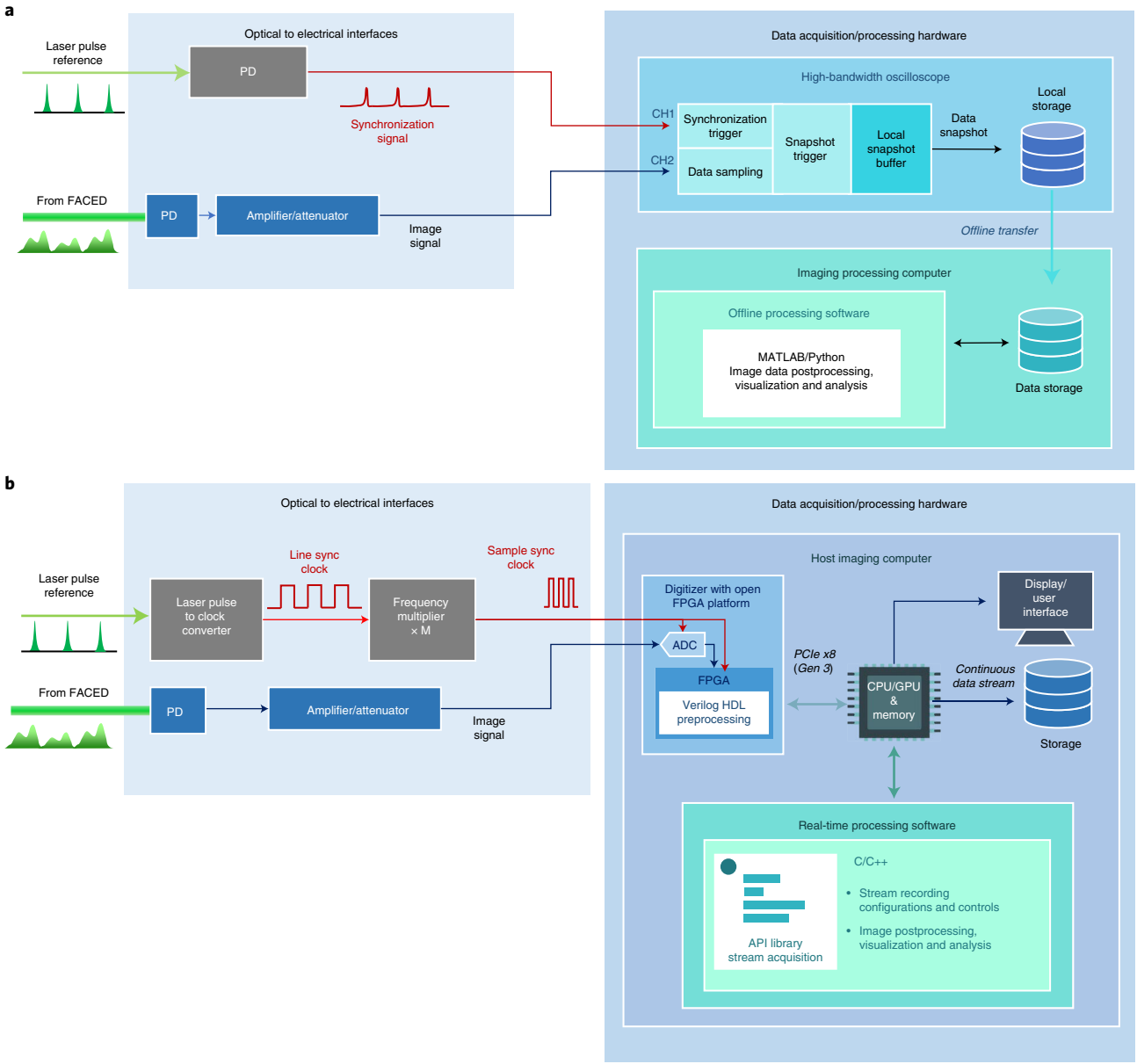

Fig. 8 | Data acquisition and image processing. a,**b**, Flow charts of the data acquisition and image processing procedures based on the high bandwidth oscilloscope (**a**) and the custom FPGA system (**b**). PD, photodetector.

31 To Implement data acquisition and processing, turn on the oscilloscope and initialize the suitable parameters (sampling rate = 10–80 GS/s, Trigger mode, Display Channel: CH1 and CH2, and/or CH3). Set the suitable data recording length (preferably three to five times of the repetition period of the pulsed laser) and the trigger threshold (75% of the peak power of the laser pulse) to characterize the actual laser repetition rate and the temporal separation between neighboring virtual sources.

32 Connect the FACED image signal (from PD/PMT) to channel 2 (CH2) of the oscilloscope. To implement multimodal FACED imaging, connect the additional image contrast signal to channel 3 (CH3). Note that an additional electronic amplifier or attenuator might be required to adjust the signal power level before being connected to the oscilloscope. Then, connect the laser trigger signal to channel 1 (CH1) of the oscilloscope.

33 Install MATLAB in the operating system of the oscilloscope. Load the custom script for data acquisition to MATLAB (see Supplementary Software under the folder 'oscilloscope_faced_imaging'). Note that other programming software could also be used to control the oscilloscope and perform image processing.

34 Open the custom program and input suitable settings, including the laser repetition rate, the temporal separation between neighboring virtual sources, number of channels used in the oscilloscope (when multimodal imaging is needed), file name for data storage and number of data-trace captured in one file.

35 Now set an even longer data recording length and an appropriate voltage reference level (for edge triggering) in the oscilloscope (4MPt) such that the whole data window of (at least) a single cell in microfluidic flow or a single 2D image frame can be displayed on the oscilloscope. Run the MATLAB script for data capture and display from channel CH2, and/or CH3. At this point, the oscilloscope is ready for optimizing the optical alignment of the system as well as characterizing the general imaging performance. After optimization, stop displaying the 2D reconstructed image and start the data capture process.

36 If data storage is needed, transfer the data to the computer workstation for offline post-image processing (Fig. 8).

37 Use an offline image processing program (same MATLAB script as Step 33) to reconstruct the 2D image by digitally stacking the raw line-scan data (Fig. 4). In this approach, the position of SOL of each line scan is first estimated by the peak search of the autocorrelation of the data trace. However, since the internal sampling frequency of the oscilloscope is completely independent of the input pulse frequency, it is common to observe an arbitrary sample position shift between the SOL on each line and the actual sampling position. The program, therefore, adopts a custom optimization algorithm to search for the actual 'SOL' position and resample the signal trace. While this may not cause very severe distortion (pixel shift) on the resulting image when using an oscilloscope with a very high sampling rate, the pixel misalignment will become more prominent as a lower sampling rate is used. The program then performs additional image processing steps, e.g., low-pass filtering, background normalization, and interpolation for image visualization and data analysis.

Setup of custom FPGA system ● Timing 14 d

▲ **CRITICAL** To handle continuous high-quality FACED image acquisition, a digitizer capable of satisfying the high analog bandwidth, sampling rate and precision requirements imposed by the source image signal must be used. This protocol takes the Teledyne SP Devices ADQ7DC-PCIe as an example of the digitizer system to meet these requirements, as well as taking advantage of the customizable signal processing logic within its open FPGA platform to achieve continuous image reconstruction, filtering, and segmentation for real-time image acquisition and storage. The system is equipped with four analog-to-digital converters (ADCs) operating in time-interleaved mode. It enables a combined sampling frequency of 10 GHz (see Supplementary Fig. 12 in Supplementary Manual 3 for a detailed illustration of the hardware). The actual sampling frequency required for each ADC is a quarter of the target sampling frequency (10 GHz/4 = 2.5 GHz), where the four ADCs receive phase-shifted versions of the 2.5 GHz clock with 0°, 90°, 180° and 270° phase shift, respectively. To generate the base 2.5 GHz ADC clock signal synchronized to the source laser pulse frequency (f_{pulse}), we need a module of a laser-pulse-to-clock convertor and a clock synthesizer (see the procedure described in Step 39).

38 Set up the host PC station comprising CPU, FPGA digitizer, GPU and storage with the following specifications/requirements:
- Use a motherboard that supports two or more Gen3 PCIe ×16 physical dimension slots for both the GPU adapter and the FPGA digitizer card (model: Teledyne SP Devices ADQ7DC-PCIe). It should electrically support at least Gen3 PCIe ×8 lanes on both the GPU and ADQ7 digitizer
- Use a CPU with at least four physical cores to accommodate the multithreaded data access and processing during data acquisition
- Equip the system with M.2 NVMe SSD storage capable of at least 3 GB/s continuous data write performance

39 Generate the line clock and sample clock using a laser-pulse-to-clock convertor and a clock synthesizer (Fig. 8b). This step is required later for ADC synchronization and image reconstruction in the FPGA digitizer. We note that there are different commercially available options of laser-pulse-to-clock convertor and clock synthesizer. In practice, the laser-pulse-to-clock convertor can be realized by using a pulse delay generator, which should have a sufficient bandwidth to detect the reference laser pulse train, large tuning range of pulse delay (from tens of ps to beyond 1 s) and high pulse delay resolution (tens of ps). The clock synthesizer should be able to generate high-frequency (>1 GHz), low-noise sample clock signal, which is fed to the digitizer (i.e., ADQ7) (Fig. 8b). As an example, here we chose a pulse delay generator with an integrated photodiode module (Aerodiode) and frequency multiplier (model Valon 5009 clock synthesizer + PS6V-1 Power Supply Kit), which

meets the above requirements for clock generation. The setup for this line clock generator includes the following three key substeps.

- Perform initial setup for the line clock generation, which employs a pulse delay generator with a photodiode module to convert the laser pulses into an electrical square wave clock signal (Supplementary Fig. 7 and Supplementary Manual 2)

  ▲ **CRITICAL STEP** Ensure that the pulse delay generator's hardware is configured to generate 1 V output signal. Power on the module, and configure the settings according to Supplementary Manual 2. Check the output signal through an oscilloscope to confirm that the output waveform has the correct square with an amplitude of 1 V and a duty cycle of ~50% (Supplementary Figs. 8 and 9).
- Feed the output clock signal from the line clock generator to a frequency multiplier. Signal connections and configurations for the modules used in this protocol are detailed in Supplementary Fig. 10, and Supplementary Manual 2. Connect the output clock signals of the frequency multiplier (Source 1 or Source 2 output of the Valon 5009 clock synthesizer) to the CLK input of the ADQ7 digitizer (Supplementary Fig. 11)
- Determine actual ADC clock frequency (f_{ADC}) by $f_{ADC} = M \times f_{pulse}$, where an integer frequency multiplying factor M (Fig. 8b) can be derived by M = Round (2.5 GHz/f_{pulse}). Although the resulting f_{ADC} may not be exactly 2.5 GHz, the ADCs are capable of tolerating the slight mismatch such that the required synchronization is achieved

  ▲ **CRITICAL STEP** Follow the settings according to Supplementary Manual 2, and check that it has successfully locked to the desired output frequency (the blue LED indicator next to the output source should light up solidly with stable brightness).

  ? TROUBLESHOOTING

40 Set up the FPGA digitizer (model Teledyne SP Devices ADQ7DC-PCIe) by first connecting the photodiode or PMT signal to the Input X (single channel mode) on the ADQ7 by the SMA cable (Supplementary Fig. 11). Note that there is also a two-channel mode where the four ADCs are divided into two sets of time-interleaved ADC pairs for two independent inputs. This allows a single ADQ7 to simultaneously record image signals from two independent sources, e.g., from two different imaging modalities. The sampling clock remains the same at 2.5 GHz as the single-channel case. However, the effective sampling frequency for each channel is now halved to 5 GHz.

▲ **CRITICAL STEP** The voltage level of the signal must be checked and limited to within ± 1 V using an attenuator to prevent damaging the sensitive ADCs in ADQ7.

? TROUBLESHOOTING

41 After the hardware setup, implement the custom logic into the custom FPGA system as described in the following FPGA data acquisition logic and image processing pipeline. It consists of three key stages:

- *Perform data sample synchronization and parallelization*: the ADQ7 digitizer generates a set of phase-shifted clocks at 2.5 GHz for the time-interleaved ADCs (Supplementary Manual 3). The structure of the clock paths and relevant hardware is illustrated in (Supplementary Fig. 12). The base 2.5 GHz clock is also used to synchronize all the real-time data/image processing within the FPGA. However, as the maximum operating frequency of the FPGA fabric is considerably lower than 2.5 GHz, a set of hardware serial-to-parallel converters are used to convert four sets of time-interleaved serial streams into the data blocks of 32 parallel samples. Since the effective sampling frequency is 10 GHz, the actual operating frequency needed to continuously handle 32 parallel samples per clock cycle is given by 10 GHz/32 = 2.5 GHz/8 = 312.5 MHz. The clock is derived from the base 2.5 GHz clock using on-chip clock management hardware as shown in Supplementary Fig. 13.
- *Implement line synchronization, data stream filtering and data reduction* (User Logic 1): process the synchronized parallel samples by the 'User Logic 1' block where the custom logic can be defined here to modify the internal line trigger for later 2D image reconstruction in the following User Logic 2 module. Any 1D signal processing /filtering can also be applied here such as finite impulse response (FIR) filters. Configure the 'Sample-skip' block, which is immediately after the User Logic 1 block, via the application programming interface (API) on the host PC to allow the samples between step size of powers of 2 to be discarded (Supplementary Fig. 12). For example, when the step size is set to 2^0, no samples are discarded; for 2^1, one sample is discarded per step; and for 2^2, three samples are discarded per step. This is particularly useful when certain signal averaging schemes are included in User Logic 1 to reduce data size and thus relax the throughput requirement in all the subsequent processing and storage stages. Apply external synchronization

through the TRIG or SYNC ports on the ADQ7 as a frame trigger (Supplementary Fig. 12) to synchronize the collection of lines (2D frame). The external frame trigger is particularly useful on systems that utilize galvo mirror scanners where each scan corresponds to a 2D frame that must be synchronized with the FPGA for correct image frame alignment and processing.

- *Implement the 2D image reconstruction and image processing/filtering* (User Logic 2) *with (a) predefined trigger period and line length, (b) external synchronization or (c) real-time segment/region-of-interest (e.g., cells) detection from the 2D image data stream* (see details in Supplementary Manual 3): for real-time segmentation, the algorithm identifies lines of interest by detecting the gradient of pixel values between adjacent lines. This can be implemented in the User Logic 2 of the FPGA within ADQ7 using a minimal amount of on-chip memory and basic arithmetic blocks. The main principle of the real-time region/segment detection hardware is described in Supplementary Fig. 14. A reference design of the above image reconstruction, filtering, data reduction and region-of-interest detection can be found in Supplementary Software under the folder 'adq7_ul1_ul2_roi'. Due to license restrictions, the repository contains only the portion of user-customizable source code in Verilog hardware description language (HDL).

  ▲ **CRITICAL STEP** You must obtain the appropriate base ADQ7 FPGA development kit project from Teledyne SP Devices with a valid license, and then replace the source code in the base project with the provided source code accordingly to compile the actual FPGA firmware. After a complete compilation within *Xilinx Vivado*, the results will be presented with a 'Worst-case Negative Slack' (WNS). This indicates the timing slack of synchronous logic within the implemented FPGA hardware. A positive value of WNS indicates that the implemented design has passed all timing requirements. However, if a certain combinatorial logic path within the design is too long, the WNS may become negative (fails timing requirements) and may not operate correctly. To fix the issue, the users must modify the design to reduce relevant path length and rerun the compilation until WNS is positive.

  ▲ **CRITICAL STEP** The main workflow of the digitizer hardware and custom logic implementation with the FPGA is summarized in Supplementary Figs. 12–14 where data samples from the ADCs are first synchronized and parallelized, then processed in two stages of the user-customizable logic block (User Logic 1 and User Logic 2). The data are finally sent to the host computer via the PCIe interface. The details and setup of each stage are described in Box 2.

42 To start data acquisition and transfer by FPGA to the host PC for image postprocessing and data storage, set the user-defined parameters in the PC including the trigger period, and the line length (record length) for 2D frame raster scanning application. Use the external trigger to be the SOL/EOL, or set the threshold for the applications where the line length is unknown, i.e., 1D flow imaging.

System calibration and fine-tuning ● Timing 3–4 d

▲ **CRITICAL** We recommend checking optimization of the scanning beam quality (e.g., minimizing the beam profile aberration) through fine-tuning of the imaging optics and FACED module prior to each imaging experiment.

43 Repeat Step 27A(iv) or 27B(v), i.e., to place a glass coverslip or a plane mirror on the sample stage to reflect scanning foci profile onto the camera (CAM) and also transmit the profile through the second objective lens (OBJ2). Check the spatial profile of the foci at CAM.

44 Translate the glass coverslip or mirror on the sample plane along the axial direction (i.e., beam propagation direction). Check if the scanning foci profile exhibits astigmatism, i.e., the smallest focal spot size in fast axis and slow axis are not on the same axial plane. If the astigmatism is substantial (displacement of the focal plane of y and x is larger than the focal depth), add a cylindrical lens with a long focal length (e.g., 200–1,000 mm) at any position along the illuminating path to compensate for astigmatism.

45 Further fine-tune the FACED mirror pair and the adjustable slit (on CP1) to optimize the beam quality of the scanning foci by repeating Steps 19–21. Examine the foci resolution/density (along the fast axis) and FOV guided by the design specifications (as shown in Fig. 7).

46 Check the temporal profile of the scanning foci by using the PD that is connected to the oscilloscope (Steps 29–32). Carefully adjust again the tilt (yaw) and pivot (pitch) angles of the FACED mirrors to obtain a smooth temporal profile (as shown in Fig. 9a) with the targeted number of virtual sources. Finely adjust the aperture size at CP1 to ensure no overlap between adjacent line scans.

Box 2 | Sample preparation

In this box, we describe how to prepare samples for system characterization and two contrasting applications of FACED, 1D line scanning in microfluidic flow and mouse brain imaging.

Procedure

(A) **Sample preparation for characterizing fluorescence PSF ● Timing 2 d**

(i) Dilute 100 μl of fluorescent Nile red particles solution (mean diameter 0.5 μm, concentration 1% wt/vol) in deionized (DI) water to get a 1:99 ratio.

(ii) Dilute 100 μl of the solution in Step (i) in DI water to get a 1:99 ratio again.

(iii) Place the solution in Step (ii) in a sonicating water bath for 10 min. This can break the clusters of beads so that single beads can be easily found on the final sample slide.

(iv) Dilute 100 μl of the solution in Step (iii) to get a 1:99 ratio with 90 % DI water and 9% ethanol (70%).

(v) Use a Mini PAP Pen to draw a circle on a coverslip. After the coverslip is completely dried, add 100 μl of the final diluted solution onto the circled area of the coverslip. A small amount of diluted 5 μm microspheres solution can be added for finding the surface of the coverslip.

(vi) Dry the coverslip under room conditions overnight.

(vii) Add a droplet of ProLong Gold Antifade Mountant onto the microscope slide, and mount the microscope slide onto the coverslip.

(viii) Dry the sample slide under room conditions overnight.

(B) **Microfluidic channel fabrication ● Timing 2 d**

▲ **CRITICAL** Fabricate the microfluidic channel that is custom designed for the targeted application at least 1 d before. The microfluidic channel is fabricated by curing polydimethylsiloxane (PDMS) on a silicon wafer mold that is prepared by soft lithography with custom microfluidic design[23].

(i) Clean the premade silicon wafer with distilled water once, and dry it with air blow.

(ii) Mix the PDMS precursor (Dow Corning, SYLGARD 184 Silicone Elastomer kit) with the corresponding curing agent at a ratio of 10:1, and pour the mixture onto the silicon wafer that is wrapped by an aluminium foil as a mold.

(iii) Put a custom-made acrylic block on the mixture that covers the imaging region of the channel to control the height of the imaging section of the microfluidic chip.

(iv) Degas the mixture in a pressure chamber to minimize the air bubbles in it.

(v) Cure the mold in the oven at 65 °C for 2 h.

(vi) Carefully extract the cured PDMS block from the silicon wafer with a knife.

(vii) Punch a pair of holes on the two ends of the cured PDMS block by using a biopsy punch (Integra LifeSciences, Miltex 33-31 AA). These two holes are used for inserting the tubings as the inlet and outlet of the microfluidic channel, respectively.

(viii) Clean the cured PDMS block and the glass slide (thickness 0.17 mm) with distilled water and filtered air blow. Expose them to oxygen plasma (Harrick Plasma, cat. no. PDC-002).

(ix) Stack the cured PDMS chip with the glass slide that is bonded together via surface activation. Put the entire chip into an oven at 65 °C for 30 min to strengthen the bonding.

(x) Carefully insert the plastic tubing (Scientific Commodities, cat. no. BB31695-PE/2) into the punched holes with UV glue applied to fill the gap.

(xi) Store the fabricated channel in a dry and clean place.

(C) **Sample preparation for 1D flow imaging with fluorescence imaging ● Timing 4–6 h**

▲ **CRITICAL** If appropriate, cells should also be stained with a suitable fluorescence dye if required for fluorescence imaging.

(i) Culture the breast cancer cells MDA-MB231 and MCF7 in the corresponding culture medium in an incubator with 5% CO_2 under 37°C.

(ii) Remove the medium, and rinse the cells with 3 ml PBS.

(iii) Add 3 ml of 0.5% Trypsin-EDTA (Gibco, cat. no. 25200072), and incubate the cells for 3 min at 37 °C.

(iv) Add 4 ml of culture medium to stop the action of trypsin.

(v) Centrifuge the mixture at 201*g* at 20 °C for 5 min. Discard supernatant.

(vi) Add 1 ml of culture medium to the cell pellet. Count the cells with the hemocytometer.

(vii) Transfer 1×10^6 cells to another test tube, and add culture medium to make the total volume of the suspension 1 ml.

▲ **CRITICAL STEP** Sample fluid must contain an appropriate cell concentration.

(viii) Dilute 1 μl of Vybrant DyeCycle orange stain (Invitrogen, cat. no. V35005) in 9 μl PBS.

(ix) Add 1.5 μl of the diluted stain into the 1 ml cell suspension. Incubate the cells for 30 min at 37 °C. The stained cells are then ready for imaging flow cytometry experiments. The cells can be stored in an incubator with 5% CO_2 at 37 °C for no more than 1 h prior to being run.

(D) **Sample preparation for mouse brain imaging ● Timing 2–4 h**

▲ **CRITICAL** Prepare the mouse for virus injection and cranial window implantation in the primary visual cortex (V1) at least 2 weeks before in vivo imaging. We followed a protocol for virus injection, and cranial window implantation in V1 can be found elsewhere[52]. Brief details of the procedure we used are below:

(i) Anesthetize mice using isoflurane (1–2% by volume in O_2), and give the analgesic buprenorphine (subcutaneously, 0.3 mg per kg of body weight). Fix the head of the mice in a stereotaxic apparatus (David Kopf Instruments, Model 1900).

(ii) Make a 3.5 mm diameter craniotomy over the left V1 (center: 3.4 mm posterior to Bregma; 2.7 mm lateral from midline) with the dura left intact.

(iii) Perform virus injection using a glass pipette (Drummond Scientific) with a 15–20 μm inner diameter and beveled at 45°. The pipette is backfilled with mineral oil. Insert a fitted plunger controlled by a hydraulic manipulator (Narishige, MO10) into the pipette. Use it to load and gently inject viral solutions (voltage indicator: AAV2/9.syn.ASAP3-Kv, 1.55×10^{12} GC ml^{-1}) into the brain (~200–400 μm below pia). Three to six sites with 300–500 μm space between adjacent sites are injected with the viral solution (30 nl per site).

(iv) After viral injections, embed an optical window made of a single coverslip (Thermo Fisher Scientific, no. 1.5) in the craniotomy and seal in place with dental acrylic.

(v) Tightly attach a titanium headpost to the skull with cyanoacrylate glue and dental acrylic.

▲ **CRITICAL** In vivo imaging should be performed 2 weeks after the craniotomy to ensure that inflammation has largely subsided. Good cranial window and virus expression are essential for high-quality data collection. For imaging head-fixed awake mice, 1 week habituation for head fixation is required to minimize stress-induced motion.

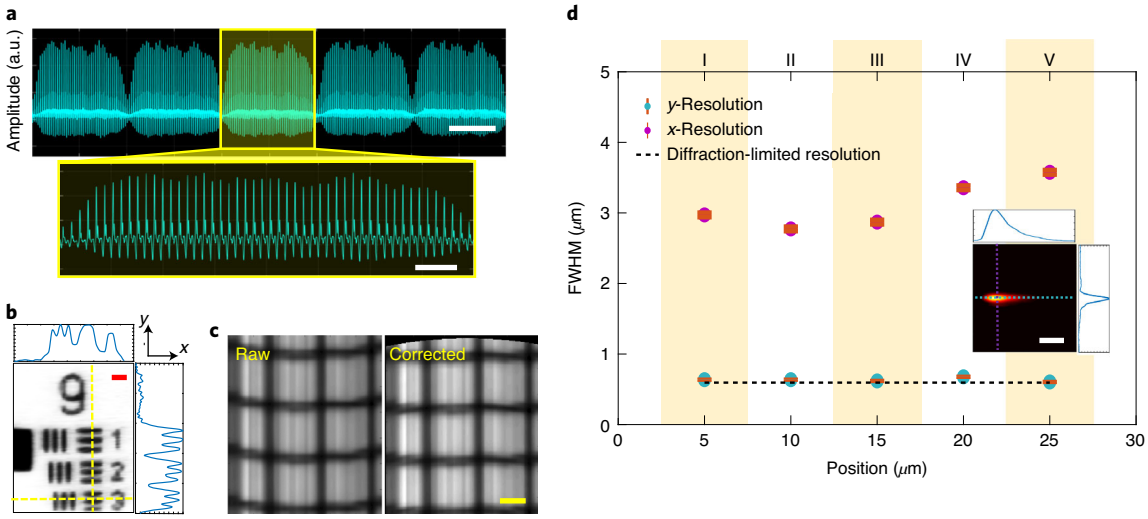

Fig. 9 | Characterization of basic FACED imaging performance. a, A typical raw time trace of (top) five FACED line scans and (below) a zoomed-in view showing individual virtual sources generated by FACED. Scale bar, 25 ns (top); 5 ns (bottom). **b**, FACED image of a USAF1951 target (FACED configuration: $N = 50$, FOV = 20 μm). Scale bar, 2 μm. **c**, Raw and corrected image of distortion grid target image captured in Step 57 (FACED configuration: $N = 50$, FOV = 30 μm). Scale bar, 5 μm. **d**, PSF measurements of the fluorescence beads ($n = 10$ for each of the five regions along the FOV) captured by the one-photon fluorescence FACED imaging system averaged by 2,000 line scans (FACED configuration: $N = 50$, FOV = 30 μm). In this plot, the average FWHM along the fast (x) and slow axis (y) are extracted from each of the five regions along the FOV (I) 2.5–7.5, (II) 7.5–12.5, (III) 12.5–17.5, (IV) 17.5–22.5 and (V) 22.5–27.5 μm. Error bars show standard deviation from ten beads. (Inset) A representative measured PSF and its line profile. Scale bar, 2 μm.

Characterization of the imaging performance ● Timing 5–6 d

Measuring the spatial resolution by using a USAF resolution target

47 Carefully mount the resolution target onto the sample stage. Use the objective (OBJ1) to coarsely focus the USAF target and search for the Group 9 elements by translating the sample stage, monitored by the camera (CAM).

▲ **CRITICAL STEP** The front surface of the target should face toward the objective (OBJ1). If the detection objective is a water-dipping type, add a drop of water onto the backside of the target.

48 Turn on the oscilloscope (by following Steps 29–32), and adjust the time window so that only a single line scan is displayed on the screen.

49 Control the motorized actuator of the sample stage to move along the slow axis for a range (total number of line scans) defined by a user-defined number of line (e.g., 200 steps with a step size of 0.2 μm), and capture the 1D line trace for each step using the oscilloscope.

50 Repeat Step 49 for different steps along the axial depth to obtain the optimal focus position.

51 Reconstruct the 2D image by stacking the 1D line traces (Fig. 9a) (see Step 37 for line-scan alignment), followed by selecting all the peaks (corresponding to the foci) along each line scan; background normalization and data interpolation along the fast axis.

? TROUBLESHOOTING

52 Measure the smallest resolved resolution from the image (Fig. 9b).

Characterizing the distortion of the FACED image by using a grid distortion test target

53 Follow Step 47 to mount the distortion target onto the sample stage. Use the photodetector (PD) (Fig. 6) for image capture.

54 Control the motorized actuator to translate in the slow axis for 1 mm at 0.1 mm/s and acquire line scan traces by using the custom FPGA system (which should be set up in Steps 38–40). Repeat Steps 41 and 42 to continuously capture the signal with a predefined line length with predefined trigger period.

▲ **CRITICAL STEP** Line skip (e.g., three-line skip (see Step 41)) might be necessary during recording to ensure continuous capture for a given data storage (e.g., a maximum of 16 GB data would allow a scan range of ~60 μm along the slow axis, given a translation speed of 0.1 mm/s).

55 Repeat Step 54 for different scanning positions along the axial depth to obtain the optimal focus position.

56 Follow Step 51 for image reconstruction. It should be noted that it is often necessary to perform additional line averaging so that the resolution will be 1 μm along the slow axis to minimize the

motion artifacts induced by the motorized actuator. Then perform data interpolation along the slow axis.

57 Check that distortion of the line scan can be visualized by the resultant image, and correct the distortion through proper image transformation (e.g., affine transformation) (Fig. 9c). After the correction, measure the FOV guided by the grid size defined in the target.
? TROUBLESHOOTING

Characterizing the resolution of FACED fluorescence imaging by microsphere

58 Mount the sample slide (see step A in Box 2) carefully onto the sample stage, and adjust the height of the sample stage by locating where the microbeads in focus. Use the PMT for fluorescence image capture.
▲ CRITICAL STEP If the objective is a water-dipping type, add a drop of water onto the backside of the slide.
? TROUBLESHOOTING

59 Follow Step 49 or 54 for controlling the motorized actuator and line scan capture. Note again the scan range along the slow axis is influenced by the available data storage, amount of optional line skip (see Step 41 and Supplementary Fig. 13) and the moving speed of the sample stage (e.g., in this case, with a three-line-skip routine, the scan range is ~660 μm for sample stage moving at 1 mm/s).

60 Repeat Step 59 for different scanning positions along with different axial depth and across the lateral positions.

61 Follow Step 51 to reconstruct a raw 2D image showing the point spread function (PSF). Then, perform line averaging (e.g., on every 2,000 lines) along the slow axis to enhance the SNR of the measured PSF.

62 Locate the peaks of fluorescent PSF in the image, and measure the full-width half-maximum (FWHM) along both the fast axis and slow axis.

63 Characterize the statistics of the PSF (mean and standard deviation of FWHM) across the line scan (Fig. 9d). As a side note, for applications where quantitative lifetime measurement is needed, the PSF should also be measured with nonfluorescent nanoparticles. Note that the resolution in the fast axis is strongly influenced by the fluorescence decay profile (Fig. 9d).

Sample preparation and mounting ● Timing 8 d

64 Prepare and mount the samples under the microscope. Required preparation steps vary depending on the specific sample properties (e.g., in vitro samples (adherent or suspended cells), in vivo samples). Here we focus on two key applications. Follow option A for 1D line-scan imaging in microfluidic flow for cytometry, or option B for 2D in vivo 2PFM imaging of living mouse brain.

(A) **1D line-scan imaging in microfluidic flow**

(i) Fabricate an appropriate microfluidic channel at least 1 d prior to imaging. Microfluidics channels can be custom designed for the targeted application; we describe in detail how to make the channel we used in the experiment of cell flow imaging in step B in Box 2.

(ii) Prepare the sample fluid with appropriate cell concentrations and stain with suitable fluorescence dye if used for fluorescence imaging as described in step C in Box 2.

(iii) Mount the microfluidic channel on the sample stage with care, and adjust the height of the sample mounting stage until the microfluidic chip is in the middle between the illumination and detection objective (OBJ1 and OBJ2). Flip the mirror FM to reroute the illumination from the LED mounted in Step 27A(vi) to the microfluidic chip. Adjust the axial position of the sample mounting stage to bring the image of the microfluidic channel into sharp focus on the camera (CAM). Adjust the lateral position of the microfluidic channel so that the line scanning beam is located at the imaging position that is marked on the chip.

(iv) Unflip the mirror (FM) so that the line beam is now projected onto and detected by the photodetector (PD) that is connected to the high-speed oscilloscope.

(v) Inject the buffer solution into the microfluidic channel. Observe the displayed waveform on the oscilloscope, and adjust the axial position of the detection objective (OBJ2) until a temporal profile shape is optimized (as calibrated in Step 46) and its intensity is maximized. Usually, iterative tuning of the detection objective and the photodetector along all three dimensions is required in this optimization step.

(vi) Inject the sample fluid into the microfluidic by using a syringe pump (Longerpump, cat. no. LSP01-1BH) at a steady flow rate according to the design of the channel. The example microfluidic channel platform design we provide with this protocol is designed for inertial focusing operation, i.e., the chip is designed to optimize the balance between the inertial lift force and the viscous drag force (the linear speed required for achieving inertial focusing in the channel is typically in the order of 1 m/s).

(vii) Run the program on the oscilloscope that displays the reconstructed image in real time (see Steps 31–35). Note that the displayed frame rate is much slower than the actual frame rate. Finely adjust again the axial position of the sample stage to obtain the sharp images of the sample, then start the data capture.

(B) **2D in vivo 2PFM imaging of living mouse brain**

(i) Fix the mouse on a dual-axis goniometric stage (Thorlabs, cat. no. GNL20) with the titanium head-post (see step D in Box 2). Using a goniometric stage allows the tip and tilt of the cranial window to be fine-tuned such that the surface of the cranial window is perpendicular to the beam propagation direction (i.e., optical axis) to minimize the optical aberration.

▲ **CRITICAL STEP** In the case of 2PFM imaging where a high-power laser is used, keep laser power low (<5 mW) for the initial setup (Step 64B(ii) and (iii)) to avoid excessive reflection of the cranial window during the alignment process.

(ii) Put the head-fixed mice under the objective lens (OBJ1), and bring the scanning foci profile close to the bottom surface of the cranial window (Fig. 6). Make sure the cranial window is out of focus. Then, slowly lower the objective lens (OBJ1) mounted on the piezo stage (Physik Instrumente, cat. no. P-725K094).

▲ **CRITICAL STEP** During this process, the sharp scanning foci profile should be seen twice (i.e., the scanning beam is focused right at the top or bottom surface of the cranial window) using the camera (CAM). The first corresponds to the reflection from the top surface of the cranial window, whereas the second is the reflection from the bottom surface of the cranial window.

(iii) Adjust the tilt knob of the goniometric stage to align the surface of the cranial window perpendicular to the optical axis. When the sharp scanning foci profile is at the bottom surface of the cranial window, move the sample along fast axis over a large distance (e.g., 1 mm) with the sample stage and adjust the axial position of the objective lens (OBJ1) to recapture a sharp beam profile. If required, also follow this step to align the slow axis.

▲ **CRITICAL STEP** This process allows estimation of how much the goniometer needs to be tuned to make the fast axis of the cranial window perpendicular to the optical axis.

(iv) Further lower the objective OBJ1 to the targeted depth (e.g., 300 μm) of the mouse brain. Optimize the galvo scanner. Further adjust the control voltage of the galvo, which should now be within its mid-range position, such that the line beam profile is at the center of FOV. Further verify that the entire 2D scanning profile does not wobble (viewed by CAM) when the galvo is powered.

▲ **CRITICAL STEP** When the data acquisition and processing steps are set up, larger imaging FOV can be achieved by stitching multiple 2D images taken at different locations along the slow axis (at a step size slightly smaller than the fast-axis FOV, e.g., 25 μm). Based on this image, the area of interest for high-speed voltage imaging can be found.

Data acquisition and processing ● Timing 1 d

65 After sample mounting, undertake data acquisition and processing using option A if data were acquired using a high-speed oscilloscope or option B if you used our custom FPGA and GPU high-speed computing platform.

(A) **Data acquisition and processing using a high-speed oscilloscope**. After sample mounting and focusing, repeat Steps 31–37 for data acquisition and image processing.

▲ **CRITICAL STEP** In this approach, multiple data storages are needed for the initial image snapshots, raw image data and result storage (Fig. 8). More storage access tends to be required than that needed for the total imaging/processing time, especially when handling large imaging

data sets. For large-scale and continuous time length data, we recommend using a custom FPGA and GPU high-speed computing platform as described in option B.

▲ **CRITICAL STEP** For a setup with more than one imaging module, e.g., fluorescence and phase-gradient imaging, or SHG and bright-field imaging, connect the additional PMT/HPD to channel 3 of the oscilloscope.

(B) **Data acquisition system using custom FPGA and GPU high-speed computing platform**

(i) After sample mounting and focusing, check that the FPGA system is set up as described in Steps 38–41. This setup includes connecting the laser trigger photodiode to the laser pulse to cock converter, implementing the frequency multiplier to generate sample sync clock to the FPGA digitizer, and connecting the FACED imaging signal to the input(s) on the FPGA digitizer's Input A, B (two-channel mode) or Input X (one-channel mode). Turn on the equipment implemented in the system. Make sure the correct program is loaded into the FPGA system and the host PC for the targeted imaging mode.

(ii) Set the user-defined parameters in the host PC including trigger period and line length (record length) parameter, use an external trigger for 2D frame raster scanning application, or set the threshold for unknown line length application, i.e., 1D flow imaging application. Then, start data acquisition and data transfer by FPGA to the host PC for image postprocessing and data storage, which is described in the next step.

(iii) Set up the host PC for image postprocessing and high-speed data storage with the linkage to the FPGA system by using a suitable cable, e.g., PCIe.

▲ **CRITICAL STEP** According to the Teledyne SP Device, data transfer via Direct Memory Access (DMA) between ADQ7 and CPU/GPUs through PCIe ×8 Gen 3 interface are limited to a data rate of ~6 GB/s. In addition, further limitations and overheads are imposed by the selected storage devices. Therefore, FPGA-based data reduction is necessary for continuous data transfer.

(iv) Load the software for GPU based image visualization into the host FPGA imaging platform that uses graphical APIs such as OpenGL for image visualization. Ensure that continuous FPGA data reduction described in Step 41 is applied to prevent data overflow while running the software. A basic visualization framework with OpenGL implemented in C++ by Microsoft Visual Studio for Windows 64-bit can be found in Supplementary Software under the folder 'adq7_visualisation'. Further GPU-based image postprocessing can be applied using GPU computing libraries such as OpenCV, OpenCL and CUDA from Nvidia.

(v) If additional GPU processing is used, identify the impact on throughput and the actual maximum image data rate from the ADQ7 FPGA to avoid possible data overflow for real-time GPU processing.

(vi) Optimize the data saving routine in the software according to the host computer system's specification and storage hardware to maximize actual throughput. The two key requirements of the data storage system are high sequential data write throughput and high capacity for long-term data acquisition (over 17 TB of data will be consumed in 1 h of sustained 5 GB/s data acquisition). It is recommended to adopt local storage devices within the host PC instead of relying on shared networked storage devices where sustained data write performance may not be guaranteed. To achieve both high capacity and throughput at a relatively lower cost, hard disk drives arranged in redundant array of inexpensive disks (RAID) configuration can be used. Assuming a single 4 TB hard disk drive can provide sustained 250 MB/s sequential write speed, a RAID0 setup with 20 drives (80 TB total) will have a theoretical transfer rate matching the maximum transfer rate of 5 GB/s from ADQ7 via GPU. Alternatively, a lower number of high-end SSDs can be used to achieve the same level of write performance if high capacity is not needed. Most high-end SSDs are capable of 2 GB/s write speed, and when configured in RAID0 mode with 3× SSDs, the combined throughput will be close to 6 GB/s.

▲ **CRITICAL STEP** For continuous data storage from the FPGA or the GPU, the sustained sequential data write throughput of the storage device must be greater than the FPGA or GPU data output rate.

Troubleshooting

Troubleshooting advice can be found in Table 2.

Table 2 | Troubleshooting table

Step	Problem	Possible reason	Solution
8	The line beam projected on the camera for the alignment camera is not as straight as a horizontal line	The pressure exerted by the clamp on the mirror is too high so that the mirror is bent	Loosen the clamp, and replace it with a clamp with a larger contact area
15	Some retroreflected light could leak out near the entrance *O*	The mirror FM1 is not at the optimal position for coupling the retroreflected light	Linearly translate the mirror FM1 along the mirror plane towards *O* so that the light is not clipped off at this edge of FM1. Carefully adjust the pitch and yaw rotation of the mirror pair afterward to maintain conditions (a) and (b) in Step 15
28B(iv)	PMT1 is difficult to align	The fluorescent signal is too weak	First, replace PMT1 with another light source (e.g., LED source whose emission spectrum coincides with the targeted fluorescence wavelengths). Direct the light output back through the cage system (with L9, M2 and DM1), and verify if the light can be focused onto the sample stage by the objective lens OBJ1. Once the alignment is done, replace the light source with PMT1
39	Sample clock generator (Valon 5009) fails to lock to the target output frequency	Valon 5009 has incorrect reference frequency settings	Correct Valon 5009's reference frequency settings (Supplementary Manual 2)
		Actual input reference clock signal has incorrect/unstable waveform, duty cycle and/or amplitude	Tune and correct the settings of the previous line clock generation stage
40	Poor signal amplitude and/or loss of DC/low-frequency components at the ADQ7 signal input	Poor SMA cable and/or SMA connectors	Tighten the SMA connectors or replace the SMA cable
51	The line scans are not properly aligned	The difference between the sampling time and period of a line scan	By finding the location of the peak of the cross-correlation signal (between each line with the first line), the difference between the location of the peak and the length of a single line scan is calculated. By shifting the lines by the calculated difference in pixel with respect to the first line, all the line traces will be well aligned with the first line trace
57	The reconstructed 2D image is distorted	The intrinsic curvature of FACED line scan	Perform affine/user-defined image transformation for image correction
58	Back reflections of fluorescence light go into the PMT	Back reflections from the highly reflective surfaces, e.g., a knife edge in the transmission path	Block the light path after the detection objective

Timing

Steps 1–3, designing the targeted FACED imaging modalities: 3–4 d
Steps 4–23, FACED module setup and calibration: 14 d
Steps 24–26, mechanical stabilization of FACED cavity (optional feedback stabilization) 3–4 d
Step 27, building the microscope system: 7–8 d
Step 28, installing the modality-specific add-on modules: 1 d
Steps 29–37, oscilloscope setup: 1 d
Steps 38–42, setup of custom FPGA system: 14 d
Step 43–46, system calibration and fine-tuning: 3–4 d
Steps 47–63, characterization of the imaging performance: 5–6 d
Step 64, sample preparation and mounting: 8 d
Step 65, data acquisition and processing: 1 d

Anticipated results

In this section, we describe how we used this protocol to undertake three different projects. We chose to highlight these applications as they use the example setups we described in detail in the procedure and demonstrate the diversity of applications of FACED.

Deep-learning image-based single-cell analysis

Using the 1D line-scan imaging configuration (Fig. 6(I)) combined with the microfluidic platform, we performed FACED imaging flow cytometry in which phase-gradient and fluorescence (Vybrant DyeCycle, Invitrogen) images of individual cells were simultaneously captured at an imaging throughput of 77,000 cells/s. To first demonstrate the power of label-free imaging cytometry, we performed a task of cell-type classification based on a total of 34 label-free morphological parameters from each single-cell phase-gradient image. These features included cell size, shape and subcellular texture (Supplementary Note 1). This high-dimensional morphological profile enabled two different breast cell types (MDA-MB231 and MCF7 cells) to be distinguished (Fig. 10a). We further quantified the classification performance by employing a deep neural-network model[47] (Supplementary Fig. 15a) with the label-free features as the network inputs. The overall accuracy was as high as 93.6% (Fig. 10a).

Subtle changes in cell morphology can also be detected by deep learning and can be used to determine biologically relevant progressions including diseases[48]. Here we demonstrate the use of FACED imaging flow cytometry for inferring cell cycle progression based on label-free phase-gradient images. We first employed the raw phase gradient and fluorescence images of individual MDA-MB231 cells as the inputs to train a convolutional neural network based regression model (Supplementary Fig. 15b) for predicting the DNA content (Fig. 10b). Here, the integrated fluorescence intensity of individual fluorescence images was used as the ground truth for training. Watson pragmatic fitting was then performed on the statistical distribution of the output fluorescence intensity to predict the fractions of cells in each of the cell cycle phases (the G1, S and G2/M phases). This regression model predicts the DNA content with Pearson's correlation $r = 0.715$ (Supplementary Fig. 16a). For better visualization, we employed the label-free phase-gradient features to reconstruct the cell cycle progression (Fig. 10b). The predicted proportions of the three phases, i.e., G1, S and G2/M were consistent with the proportions determined by the fluorescence DNA label (Supplementary Fig. 16b).

SHG imaging flow cytometry

Using SHG imaging, we imaged microalgae (*Scenedesmus*) in microfluidic flow, similar to the configuration described in the previous section but with the setup implementation shown in Fig. 6(II). The SHG signal was generated primarily from the cellulose in the cell wall and the starch grains in chloroplast[49]. The line scan rate of this setup was 80 MHz, which is the laser original repetition rate without the need for pulse picking. FACED cavity was adjusted to have a temporal delay of 225 ps between individual modes with a total of ~60 virtual sources, which covered a FOV of ~30 μm along the FACED axis. *Scenedesmus* is rich in starch and lipid and is used for biofuel production[50]. We cultured *Scenedesmus* for 48 h in a 14 h/10 h day/night cycle in two different culture media, i.e., BG-11 and BG-11(-N). The key difference between the media is that BG-11(-N) lacks nitrogen and could induce the accumulation of starch in microalgae[51]. The microalgae from both batches were loaded in a microfluidic channel (with a channel cross-section of 30 × 60 μm within the imaging region) at a flow speed of 0.1 m/s, which provided an imaging throughput of ~5,000 cells/s. Such a flow rate can be further adjusted (slowed down) to maximize the SHG signal. Apart from the SHG contrast, we also captured the bright-field image of the microalgae, with each row in the image being the average of 40 raw line scans. To generate the SHG images, we implement a time-gated photon counting approach. In this detection scheme, a time window (set to be the time delay between two neighboring virtual sources τ) (gate) is selected within the impulse response of the hybrid photodetector (i.e., 225 ps as shown in Supplementary Fig. 17). Along the fast axis, each resultant SHG image pixel was generated by binning the photon counts within the time window of τ. We note that this scheme can improve the temporal response. On the slow axis, each pixel was formed by binning 80 raw line scans (i.e., the flow direction) (Fig. 10c). We also analyzed the normalized cell area (CA), normalized SHG area (SA) and the ratio of the two parameters on the SHG and bright-field images (Fig. 10c). This demonstrated that *Scenedesmus* cultured in nitrogen-deficient medium has a stronger SHG signal and the mean value of the ratio of CA/SA is statistically higher (P-value < 0.005 at the Ci of 95% and

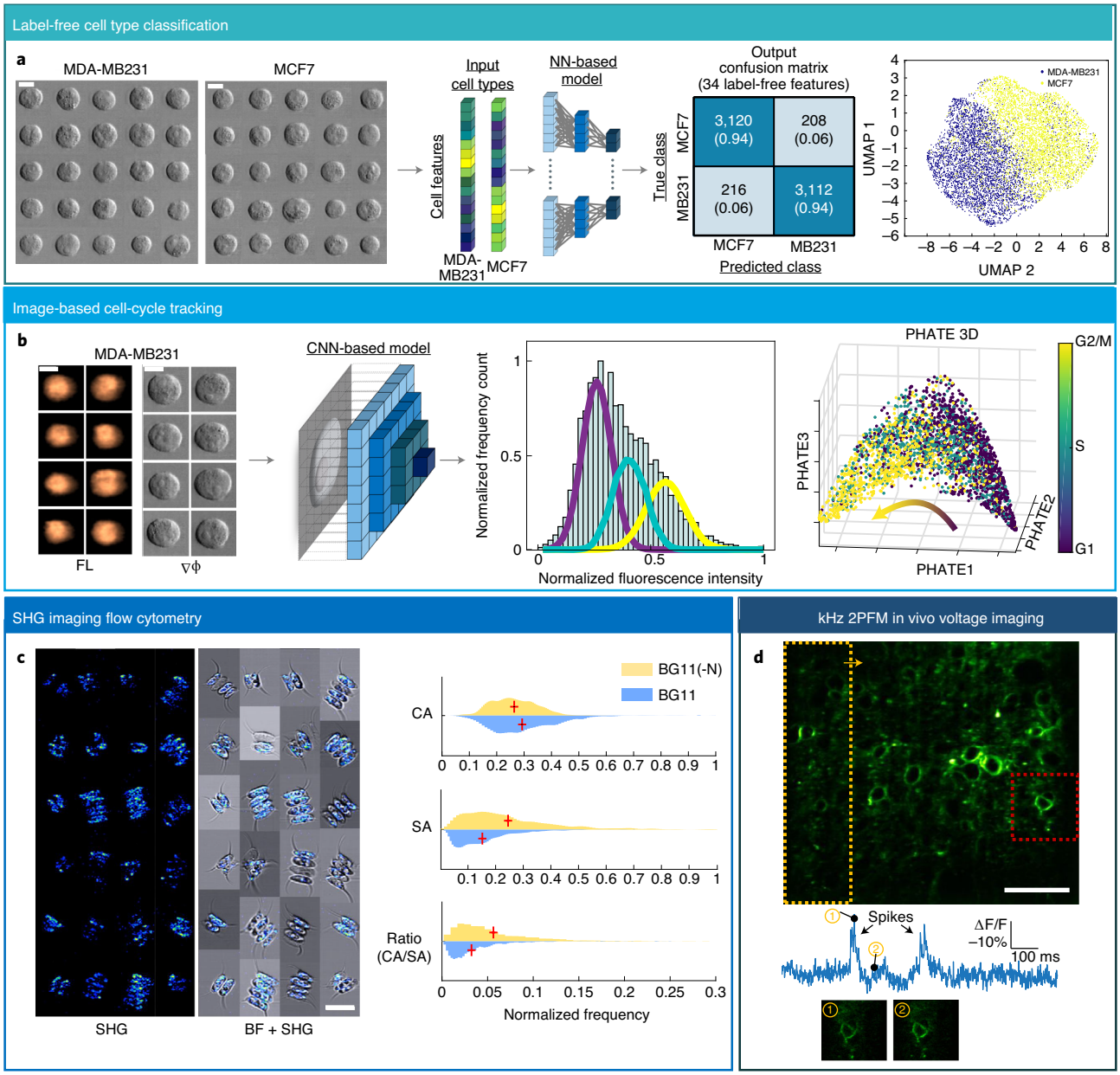

Fig. 10 | Applications of FACED imaging. a, Label-free image-based cell-type classification: selected phase-gradient images of MDA-MB231 and MCF7 are shown. $n = 8{,}656$. Scale: 10 μm. Label-free features are extracted from the cell images, and they are input into a neural-network (NN)-based model for classification. The confusion matrix shows the high accuracy of cell-type classification. Besides, the UMAP plot (based on 10 out of 34 features (Supplementary Note 1)) also shows that the two clusters of different cell types are clearly separated. Note that details of the NN-based model can be referred to Supplementary Fig. 15a. **b**, Deep-learning label-free tracking of cell-cycle stages. Selected phase-gradient ($\nabla\varphi$) and fluorescence (FL) images of MDA-MB231 ($n = 2725$) are shown. Scale: 10 μm. The phase-gradient images are input into a convolutional NN-based regression model for predicting the DNA content of individual cells, while the integrated intensity calculated from the fluorescence images are used as ground truth for identification of cell cycle stages. Watson's pragmatic curve fitting is performed on the histogram of the predicted fluorescence intensities to predict the proportions of the cell cycle phases, i.e., G1, S and G2/M. The PHATE 3D plot is constructed based on the fluorescence labels of the cells, and cell cycle progression can be clearly visualized. Note that details of the convolutional neural network model can be referred to in Supplementary Fig. 15b. **c**, SHG imaging flow cytometry of microalgae. SHG signals and the overlay of bright-field and SHG signal of *Scenedesmus* ($n = 2{,}085$) (captured in a flow of 0.1 m/s with averaging of 80 line scans). Scale: 20 μm; laser intensity: ~1.2×10^9 W/cm^2. The extracted CA and SA segmented separately on bright-field and SHG images and the ratio of the two parameters (CA/SA) are plotted in the violin plot on the right showing that the mean value (red cross) and the overall distribution of the ratio is higher for *Scenedesmus* cultured in BG11(-N) than that in BG11 medium. **d**, kHz 2PFM voltage imaging in living mouse brain. Representative image of neurons in primary visual cortex labeled with voltage indicator, soma-targeted ASAP3-Kv. Scale: 50 μm. The image is a stitch of eight FACED image scans (yellow square) along the *x*-axis with a step size of 25 μm averaged with 50 frames. Targeted FOV (red square) for functional imaging at 1,000 fps. Laser intensity: ~1.1×10^{11} W/cm^2 (note that the peak intensity of each focus could vary depending on the optical loss in the setup, as well as dispersion compensation). Imaging depth: 125 μm. Inverted spontaneous voltage traces ($\Delta F/F$) (bottom) from neurons extracted in the image above (white arrow); Two representative images of at the peak of (1) the spike and (2) the baseline of the area in red box.

Hedge's *g* effect size of 0.66 followed the methods suggested in Nakagawa's study[51]). These results suggested there was an increase in starch accumulation in algal cells under nitrogen stress, consistent with the previous studies[51]. This demonstrates that cytometry based on SHG contrast could be useful for label-free monitoring of algal growth, with applications in biofuel and superfood production[52].

kHz voltage imaging in living mouse brain

Using the 2PFM configuration (Fig. 6(III)), we imaged neurons expressing the genetically encoded voltage indicator ASAP3 in V1 of the head-fixed awake mouse (Fig. 10d). ASAP-family indicators are currently the only groups of genetically encoded voltage indicators that have demonstrated both subthreshold and suprathreshold voltage responses in vivo with 2PFM[2]. We used a FACED microscope generating 80 pulsed foci spanning 50 μm at a line-scan rate of 1 MHz. The temporal delay between adjacent foci was adjusted to be 2 ns to minimize pixel crosstalk due to fluorescence lifetime and detector response time. Using the GM to scan the foci along the slow axis (orthogonal to the FACED-line-scan axis at 500 Hz), we could achieve a 2D frame rate of 1,000 fps by capturing the image data bidirectionally. The effective frame size was 80 × 900 pixels, where 80 was determined by the number of foci in the FACED axis whereas 900 was determined by the product of the actual frame time (unidirectional sweep time of the galvo (1 ms) minus a dead time during each sweep (0.1 ms)) and line scan rate (1 MHz). In this experiment, we also placed an additional GM (*x*-galvo) close to the existing GM (*y*-galvo) along the light path of the system such that *x*-galvo can be used to widen the FOV by tiling multiple FACED images along the fast axis (e.g., Fig. 10d). This is particularly useful for large-FOV morphological imaging. By performing FACED-2PFM imaging at the depth of 125 μm, we observed fluorescence localized in the somata of neurons in the primary visual cortex labeled with soma-targeted ASAP3-Kv (Fig. 10d).

In a typical experiment for monitoring the voltage activities of individual neurons, a region of interest is manually selected in the image to cover the cell membrane and extract the mean fluorescence intensity time trace (ΔF/F) within the region of interest, where F is the baseline fluorescence and ΔF is the fluorescence change due to the voltage activity. It is necessary to adjust the laser power to achieve the desired SNR by taking single snapshots at high speed (e.g., 1,000 fps) prior to the actual time trace recording for high-speed functional studies. Note that ASAP3 reports action potentials as inverted spikes/dips in fluorescence. In addition to ΔF/F traces, we calculate SNR traces as the ratio between ΔF (functional change) and √F (Poisson noise). This SNR trace, subsequently low-pass filtered (e.g., a 250 Hz 12th order low-pass Butterworth filter), is used for spike detection. The SNR threshold for spikes depends on the experimental conditions. A representative time trace of voltage spontaneous spiking and subthreshold activity from a neuron measured by FACED-2PFM at 1,000 fps is shown in Fig. 10d.

Reporting Summary

Further information on research design is available in the Nature Research Reporting Summary linked to this article.

Data availability

The custom codes and data used in this protocol are available in the Supplementary Software and upon request, respectively.

References

1. Pawley, J. *Handbook of Biological Confocal Microscopy* Vol. 236 (Springer Science & Business Media, 2006).
2. Villette, V. et al. Ultrafast two-photon imaging of a high-gain voltage indicator in awake behaving mice. *Cell* **179**, 1590–1608 (2019).
3. Gong, Y. et al. High-speed recording of neural spikes in awake mice and flies with a fluorescent voltage sensor. *Science* **350**, 1361–1366 (2015).
4. Regev, A. et al. Science forum: the human cell atlas. *eLife* **6**, e27041 (2017).
5. Usaj, M. M. et al. High-content screening for quantitative cell biology. *Trends Cell Biol* **26**, 598–611 (2016).
6. Pegoraro, G. & Misteli, T. High-throughput imaging for the discovery of cellular mechanisms of disease. *Trends Genet* **33**, 604–615 (2017).
7. Wu, J.-L. et al. Ultrafast laser-scanning time-stretch imaging at visible wavelengths. *Light Sci. Appl.* **6**, e16196–e16196 (2017).
8. Yan, W., Wu, J., Wong, K. K. Y. & Tsia, K. K. A high-throughput all-optical laser-scanning imaging flow cytometer with biomolecular specificity and subcellular resolution. *J. Biophotonics* **11**, e201700178 (2018).

9. Wu, J. et al. Multi-MHz laser-scanning single-cell fluorescence microscopy by spatiotemporally encoded virtual source array. *Biomed. Opt. Express* **8**, 4160–4171 (2017).
10. Ren, Y.-X. et al. Parallelized volumetric fluorescence microscopy with a reconfigurable coded incoherent light-sheet array. *Light Sci. Appl.* **9**, 8 (2020).
11. Wu, J. et al. Kilohertz two-photon fluorescence microscopy imaging of neural activity in vivo. *Nat. Methods* **17**, 287–290 (2020).
12. Barteneva, N. S. & Vorobjev, I. A. *Imaging Flow Cytometry* (Springer, 2016).
13. Tang, A. H. L. et al. Time-stretch microscopy on a DVD for high-throughput imaging cell-based assay. *Biomed. Opt. Express* **8**, 640–652 (2017).
14. Li, Y. et al. Deep cytometry: deep learning with real-time inference in cell sorting and flow cytometry. *Sci. Rep.* **9**, 11088 (2019).
15. Lau, A. K. et al. Interferometric time-stretch microscopy for ultrafast quantitative cellular and tissue imaging at 1 μm. *J. Biomed. Opt.* **19**, 76001 (2014).
16. Guo, B. et al. Optofluidic time-stretch quantitative phase microscopy. *Methods* **136**, 116–125 (2018).
17. Jin, D. et al. Large population cell characterization using quantitative phase cytometer. *Cytom. A* **91**, 450–459 (2017).
18. Guo, B. et al. High-throughput, label-free, single-cell, microalgal lipid screening by machine-learning-equipped optofluidic time-stretch quantitative phase microscopy. *Cytom. A* **91**, 494–502 (2017).
19. Merola, F. et al. Tomographic flow cytometry by digital holography. *Light Sci. Appl.* **6**, e16241–e16241 (2017).
20. Bianco, V. et al. Endowing a plain fluidic chip with micro-optics: a holographic microscope slide. *Light Sci. Appl.* **6**, e17055–e17055 (2017).
21. Mandracchia, B. et al. Holographic microscope slide in a spatio-temporal imaging modality for reliable 3D cell counting. *Lab Chip* **17**, 2831–2838 (2017).
22. Huang, D. et al. High-speed live-cell interferometry: a new method for quantifying tumor drug resistance and heterogeneity. *Anal. Chem.* **90**, 3299–3306 (2018).
23. Lee, K. C. M. et al. Multi-ATOM: ultrahigh-throughput single-cell quantitative phase imaging with sub-cellular resolution. *J. Biophotonics* **12**, e201800479 (2019).
24. Lee, K. C. M. et al. Quantitative phase imaging flow cytometry for ultra-large-scale single-cell biophysical phenotyping. *Cytom. A* **95**, 510–520 (2019).
25. Ugele, M. et al. Label-free high-throughput leukemia detection by holographic microscopy. *Adv. Sci.* **5**, 1800761 (2018).
26. Mugnano, M. et al. Label-free optical marker for red-blood-cell phenotyping of inherited anemias. *Anal. Chem.* **90**, 7495–7501 (2018).
27. Karandikar, S. H. et al. Reagent-free and rapid assessment of T cell activation state using diffraction phase microscopy and deep learning. *Anal. Chem.* **91**, 3405–3411 (2019).
28. Wang, D. & Bodovitz, S. Single cell analysis: the new frontier in 'omics'. *Trends Biotechnol* **28**, 281–290 (2010).
29. Doan, M. et al. Diagnostic potential of imaging flow cytometry. *Trends Biotechnol* **36**, 649–652 (2018).
30. Chen, T.-W. et al. Ultrasensitive fluorescent proteins for imaging neuronal activity. *Nature* **499**, 295–300 (2013).
31. Marvin, J. S. et al. An optimized fluorescent probe for visualizing glutamate neurotransmission. *Nat. Methods* **10**, 162–170 (2013).
32. Kong, L. et al. Continuous volumetric imaging via an optical phase-locked ultrasound lens. *Nat. Methods* **12**, 759–762 (2015).
33. Huang, C. et al. All-optical volumetric physiology for connectomics in dense neuronal structures. *iScience* **22**, 133–146 (2019).
34. Marshall, G. F. & Stutz, G. E. *Handbook of Optical and Laser Scanning* (CRC Press, 2011).
35. Choi, S. et al. Development of a high speed laser scanning confocal microscope with an acquisition rate up to 200 frames per second. *Opt. Express* **21**, 23611–23618 (2013).
36. Römera, G. & Bechtoldb, P. Electro-optic and acousto-optic laser beam scanners—invited paper. *Phys. Procedia* **56**, 29–39 (2014).
37. Schlachter, S. C. et al. Spectrally encoded confocal microscopy of esophageal tissues at 100 kHz line rate. *Biomed. Opt. Express* **4**, 1636–1645 (2013).
38. Goda, K., Tsia, K. K. & Jalali, B. Serial time-encoded amplified imaging for real-time observation of fast dynamic phenomena. *Nature* **458**, 1145–1149 (2009).
39. Lau, A. K. S., Shum, H. C., Wong, K. K. Y. & Tsia, K. K. Optofluidic time-stretch imaging—an emerging tool for high-throughput imaging flow cytometry. *Lab Chip* **16**, 1743–1756 (2016).
40. Karpf, S. et al. Spectro-temporal encoded multiphoton microscopy and fluorescence lifetime imaging at kilohertz frame-rates. *Nat. Commun.* **11**, 2062 (2020).
41. Kubitscheck, U. (ed.). *Fluorescence Microscopy: From Principles to Biological Applications* (Wiley-Blackwell, 2013).
42. Mazumdar, A. Principles and techniques of Schlieren imaging systems (Columbia University Computer Science Technical Reports, CUCS-016-13, 2013).
43. Wong, T. T. W. et al. Asymmetric-detection time-stretch optical microscopy (ATOM) for ultrafast high-contrast cellular imaging in flow. *Sci. Rep.* **4**, 3656 (2014).

44. Chen, X., Nadiarynkh, O., Plotnikov, S. & Campagnola, P. J. Second harmonic generation microscopy for quantitative analysis of collagen fibrillar structure. *Nat. Protoc.* **7**, 654–669 (2012).
45. Sun, W., Tan, Z., Mensh, B. D. & Ji, N. Thalamus provides layer 4 of primary visual cortex with orientation- and direction-tuned inputs. *Nat. Neurosci.* **19**, 308 (2016).
46. Siu, D. M. D. et al. Deep-learning-assisted biophysical imaging cytometry at massive throughput delineates cell population heterogeneity. *Lab Chip* (2020).
47. Cox, G. C., Moreno, N. & Feijo, J. Second-harmonic imaging of plant polysaccharides. *J. Biomed. Opt.* **10**, 24013 (2005).
48. Singh, J. & Gu, S. Commercialization potential of microalgae for biofuels production. *Renew. Sustain. Energy Rev.* **14**, 2596–2610 (2010).
49. Dragone, G., Fernandes, B. D., Abreu, A. P., Vicente, A. A. & Teixeira, J. A. Nutrient limitation as a strategy for increasing starch accumulation in microalgae. *Appl. Energy* **88**, 3331–3335 (2011).
50. Nakagawa, S. & Cuthill, I. C. Effect size, confidence interval and statistical significance: a practical guide for biologists. *Biol. Rev.* **82**, 591–605 (2007).
51. Koyande, A. K. et al. Microalgae: a potential alternative to health supplementation for humans. *Food Sci. Hum. Wellness* **8**, 16–24 (2019).
52. Blasi, T. et al. Label-free cell cycle analysis for high-throughput imaging flow cytometry. *Nat. Commun.* **7**, 10256 (2016).

Acknowledgements

The work is supported by the Research Grants Council of the Hong Kong Special Administrative Region of China (grant nos. 17209017, 17259316, 17207715, C7047-16G and RFS2021-7S06), Innovation and Technology Support Programme (ITS/204/18), NIH BRAIN Initiative grants 1UF1NS107696.

Author contributions

All authors contributed to the development of the protocol and the writing of the manuscript.

Competing interests

K.K.T. and the University of Hong Kong have filed a US patent application (14/733,454) that relates to the all-optical laser-scanning imaging methods.

Additional information

Supplementary information The online version contains supplementary material available at https://doi.org/10.1038/s41596-021-00576-4.

Correspondence and requests for materials should be addressed to N.J. or K.K.T.

Peer review information *Nature Protocols* thanks Pietro Ferraro and the other, anonymous reviewer(s) for their contribution to the peer review of this work.

Reprints and permissions information is available at www.nature.com/reprints.

Publisher's note Springer Nature remains neutral with regard to jurisdictional claims in published maps and institutional affiliations.

Received: 27 October 2020; Accepted: 25 May 2021;
Published online: 2 August 2021

Related links
Key references associated with this protocol
Wu, J. L. et al. *Light Sci. Appl.* **6**, e16196 (2017): https://doi.org/10.1038/lsa.2016.196
Wu, J. et al. *Nat. Methods* **17**, 287–290 (2020): https://doi.org/10.1038/s41592-020-0762-7
Ren, Y. X. et al. *Light Sci. Appl.* **9**, 8 (2020): https://doi.org/10.1038/s41377-020-0245-8

nature research

Corresponding author(s): DBPR NP-P200399B Queenie T.K. Lai

Last updated by author(s): Apr 13, 2021

Reporting Summary

Nature Research wishes to improve the reproducibility of the work that we publish. This form provides structure for consistency and transparency in reporting. For further information on Nature Research policies, see our Editorial Policies and the Editorial Policy Checklist.

Statistics

For all statistical analyses, confirm that the following items are present in the figure legend, table legend, main text, or Methods section.

n/a	Confirmed	
☐	☒	The exact sample size (*n*) for each experimental group/condition, given as a discrete number and unit of measurement
☐	☒	A statement on whether measurements were taken from distinct samples or whether the same sample was measured repeatedly
☐	☒	The statistical test(s) used AND whether they are one- or two-sided *Only common tests should be described solely by name; describe more complex techniques in the Methods section.*
☐	☒	A description of all covariates tested
☒	☐	A description of any assumptions or corrections, such as tests of normality and adjustment for multiple comparisons
☐	☒	A full description of the statistical parameters including central tendency (e.g. means) or other basic estimates (e.g. regression coefficient) AND variation (e.g. standard deviation) or associated estimates of uncertainty (e.g. confidence intervals)
☒	☐	For null hypothesis testing, the test statistic (e.g. *F*, *t*, *r*) with confidence intervals, effect sizes, degrees of freedom and *P* value noted *Give P values as exact values whenever suitable.*
☒	☐	For Bayesian analysis, information on the choice of priors and Markov chain Monte Carlo settings
☐	☒	For hierarchical and complex designs, identification of the appropriate level for tests and full reporting of outcomes
☐	☒	Estimates of effect sizes (e.g. Cohen's *d*, Pearson's *r*), indicating how they were calculated

Our web collection on statistics for biologists contains articles on many of the points above.

Software and code

Policy information about availability of computer code

Data collection	Custom code and custom MATLAB code in supplementary software (uploaed zip file)
Data analysis	Custom MATLAB code in supplementary software (uploaded zip file)

For manuscripts utilizing custom algorithms or software that are central to the research but not yet described in published literature, software must be made available to editors and reviewers. We strongly encourage code deposition in a community repository (e.g. GitHub). See the Nature Research guidelines for submitting code & software for further information.

Data

Policy information about availability of data

All manuscripts must include a data availability statement. This statement should provide the following information, where applicable:

- Accession codes, unique identifiers, or web links for publicly available datasets
- A list of figures that have associated raw data
- A description of any restrictions on data availability

The data that support the findings of this study are available from the corresponding author upon reasonable request.

Field-specific reporting

Please select the one below that is the best fit for your research. If you are not sure, read the appropriate sections before making your selection.

☒ Life sciences ☐ Behavioural & social sciences ☐ Ecological, evolutionary & environmental sciences

For a reference copy of the document with all sections, see nature.com/documents/nr-reporting-summary-flat.pdf

Life sciences study design

All studies must disclose on these points even when the disclosure is negative.

Sample size	The sample sizes were determined by its total captured cell images and statistical analysis like effect size measures and correlation factor are calculated to ensure the sample size is sufficient.
Data exclusions	Images that are out-of-focus and blank with noise only are excluded.
Replication	Only one time of the experiment is conducted in this demonstration but similar studies are replicated in our lab with different imaging system.
Randomization	The cells were randomly extracted from the cell culture.
Blinding	the investigator was not blind to group allocation during the data acquisition and collection procedure because we need to provide the true label for the training of cell classification and study the signal difference between the chemical altered group of cell. For the neuron experiment, only neurons with significant activities were catured to demonstrating the imaging capability.

Reporting for specific materials, systems and methods

We require information from authors about some types of materials, experimental systems and methods used in many studies. Here, indicate whether each material, system or method listed is relevant to your study. If you are not sure if a list item applies to your research, read the appropriate section before selecting a response.

Materials & experimental systems

n/a	Involved in the study
☒	☐ Antibodies
☐	☒ Eukaryotic cell lines
☒	☐ Palaeontology and archaeology
☐	☒ Animals and other organisms
☒	☐ Human research participants
☒	☐ Clinical data
☒	☐ Dual use research of concern

Methods

n/a	Involved in the study
☒	☐ ChIP-seq
☒	☐ Flow cytometry
☒	☐ MRI-based neuroimaging

Eukaryotic cell lines

Policy information about cell lines

Cell line source(s)	Breast cancer cell line: MCF7 and MB231
Authentication	Cellular morphology are routinely checked during cell culture under light microscope prior to imaging experiments
Mycoplasma contamination	Preventing of mycoplasma contaminationwas done by adding antibiotic-antimycotic during cell culture
Commonly misidentified lines (See ICLAC register)	None were used.

Animals and other organisms

Policy information about studies involving animals; ARRIVE guidelines recommended for reporting animal research

Laboratory animals	Wild-type (females or males, >2-months-old, Jackson Laboratories, Black 6, stock no. 000664) mice
Wild animals	The study did not involve wild-animals.
Field-collected samples	The study did not involve any field-collected samples.

Ethics oversight	All animal experiments were conducted in this procedure according to the National Institutes of Health guidelines for animal research. Procedures and protocols on mice were approved by the Institutional Animal Care and Use Committee at Janelia Research Campus, Howard Hughes Medical Institute.

Note that full information on the approval of the study protocol must also be provided in the manuscript.